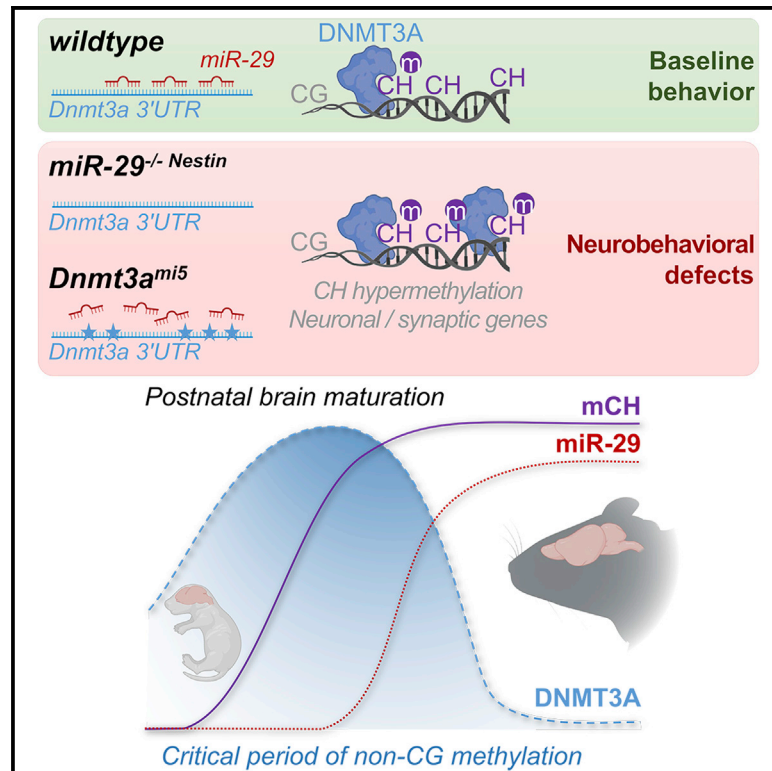


MicroRNA-29 is an essential regulator of brain maturation through regulation of CH methylation

Graphical abstract



Authors

Vijay Swahari, Ayumi Nakamura, Emilie Hollville, ..., Sheryl S. Moy, Michael E. Greenberg, Mohanish Deshmukh

Correspondence

swahari@email.unc.edu (V.S.), mohanish@med.unc.edu (M.D.)

In brief

Non-canonical CH methylation mediated by DNMT3A during neuronal maturation has been recently shown to be critical for brain homeostasis. Swahari et al. identify a key player that is critical for regulating CH methylation: the microRNA miR-29. Failure of miR-29 to regulate the expression of *Dnmt3a* leads to severe neurobehavioral consequences.

Highlights

- miR-29 is markedly upregulated during postnatal brain maturation
- miR-29 targets *Dnmt3a* to restrict its expression *in vivo* in the maturing brain
- miR-29 regulates *Dnmt3a* and mCH to control the expression of synaptic genes
- Failure of miR-29 to restrict *Dnmt3a* leads to neurobehavioral deficits



Article

MicroRNA-29 is an essential regulator of brain maturation through regulation of CH methylation

Vijay Swahari,^{1,10,*} Ayumi Nakamura,^{1,2,10} Emilie Hollville,^{1,10} Hume Stroud,³ Jeremy M. Simon,^{1,5,8} Travis S. Ptacek,^{1,8} Matthew V. Beck,¹ Cornelius Flowers,¹ Jiami Guo,¹ Charlotte Plestant,¹ Jie Liang,⁴ C. Lisa Kurtz,⁵ Matt Kanke,⁶ Scott M. Hammond,⁹ You-Wen He,⁴ E.S. Anton,^{1,2,9} Praveen Sethupathy,^{5,6} Sheryl S. Moy,^{7,8} Michael E. Greenberg,³ and Mohanish Deshmukh^{1,2,8,9,11,*}

¹Neuroscience Center, University of North Carolina, Chapel Hill, NC, USA

²Neurobiology Curriculum, University of North Carolina, Chapel Hill, NC, USA

³Department of Neurobiology, Harvard University, Boston, MA, USA

⁴Department of Immunology, Duke University, Durham, NC, USA

⁵Department of Genetics, University of North Carolina, Chapel Hill, NC, USA

⁶Department of Biomedical Sciences, Cornell University, Ithaca, NY, USA

⁷Department of Psychiatry, University of North Carolina, Chapel Hill, NC, USA

⁸Carolina Institute for Developmental Disabilities, University of North Carolina, Chapel Hill, NC, USA

⁹Department of Cell Biology and Physiology, University of North Carolina, Chapel Hill, NC, USA

¹⁰These authors contributed equally

¹¹Lead contact

*Correspondence: swahari@email.unc.edu (V.S.), mohanish@med.unc.edu (M.D.)

<https://doi.org/10.1016/j.celrep.2021.108946>

SUMMARY

Although embryonic brain development and neurodegeneration have received considerable attention, the events that govern postnatal brain maturation are less understood. Here, we identify the miR-29 family to be strikingly induced during the late stages of brain maturation. Brain maturation is associated with a transient, postnatal period of *de novo* non-CG (CH) DNA methylation mediated by DNMT3A. We examine whether an important function of miR-29 during brain maturation is to restrict the period of CH methylation via its targeting of *Dnmt3a*. Deletion of miR-29 in the brain, or knockin mutations preventing miR-29 to specifically target *Dnmt3a*, result in increased DNMT3A expression, higher CH methylation, and repression of genes associated with neuronal activity and neuropsychiatric disorders. These mouse models also develop neurological deficits and premature lethality. Our results identify an essential role for miR-29 in restricting CH methylation in the brain and illustrate the importance of CH methylation regulation for normal brain maturation.

INTRODUCTION

Although there is considerable knowledge surrounding brain development (e.g., neurogenesis, neuronal migration, and postmitotic differentiation), less is known about how the brain matures after this period and how brain homeostasis is maintained throughout adulthood. During brain maturation, widespread changes in synaptic connectivity are evident (Jiang and Nardelli, 2016; Stiles and Jernigan, 2010), and perturbations of synaptic development or maturation can result in severe neurobehavioral sequelae as seen in autism spectrum disorders (ASD), epilepsy, and schizophrenia (Bourgeron, 2015; Forsyth and Lewis, 2017; McTague et al., 2016; Toga et al., 2006).

MicroRNAs (miRNAs), which have the potential to post-transcriptionally silence hundreds of genes, are already known to modulate neurodevelopment (Petri et al., 2014; Sun and Shi, 2015) and neurodegeneration (Abe and Bonini, 2013; Juźwik et al., 2019). Accordingly, specific miRNAs that regulate neuronal activity and synaptic function in established neurons have been

identified (Dubes et al., 2019; Edbauer et al., 2010; Schrott et al., 2006; Siegert et al., 2015). However, whether there are miRNAs that are selectively induced and functionally important during postnatal brain maturation is unknown.

Several recent studies have identified a critical period during postnatal mammalian brain development during which there is a dramatic increase in the methylation of the neuronal genome at non-canonical (non-CG) CH sequences (Chen et al., 2015; Gabel et al., 2015; Guo et al., 2014; He and Ecker, 2015; Kinde et al., 2015; Lister et al., 2013; Mo et al., 2015; Xie et al., 2012). This period of *de novo* CH methylation (where H = A, C, T) starts at birth and persists for 1–4 weeks in mice and 1–15 years in humans (Lister et al., 2013). During this maturation stage, deposition of these methyl-CH (mCH) marks have been hypothesized to regulate neuronal diversity by fine-tuning gene transcription across the genome (Chen et al., 2015; Luo et al., 2017; Rizzardi et al., 2019; Stroud et al., 2017).

CH methylation is catalyzed by the DNA methyltransferase DNMT3A (Gabel et al., 2015; Guo et al., 2014). The time course



of mCH deposition in postnatal neurons is tightly controlled such that the level of DNMT3A that are elevated during early brain maturation sharply decline several weeks after birth (Feng et al., 2005; Lister et al., 2013). This decrease in DNMT3A results in a cessation in the deposition of additional mCH and may be essential for proper brain maturation (Lister et al., 2013). The importance of strict control of CH methylation is emphasized by the association of mutations in *DNMT3A*, as well as in the methyl-binding proteins that bind to mCH (e.g., MeCP2 and the MBD family), with devastating disorders of postnatal brain development, including ASD, epilepsy, and intellectual disability (Gigek et al., 2016; Liu et al., 2018a, 2018b; Lombardi et al., 2015; Tatton-Brown et al., 2014; Yuen et al., 2016). However, the mechanisms that control the repression of DNMT3A expression to regulate CH methylation during postnatal brain development have not yet been identified, and the consequences of unrestricting this critical period of CH methylation remain unclear.

Dnmt3a is known to be targeted by several miRNAs. For example, miR-370 and miR-495 regulate *Dnmt3a* expression during embryonic development and stem cell differentiation (Qi et al., 2013; Yang et al., 2014), and miR-132 and miR-143 modulate *Dnmt3a* expression in neurodevelopmental disorders and nerve injury, respectively (Miller et al., 2012; Xu et al., 2017). Additionally, miR-29 regulates *Dnmt3a* expression in multiple situations including embryonic development, cancer, and other pathologies. In particular, in the context of the nervous system, miR-29-regulated *Dnmt3a* expression has been associated with neuronal differentiation (Xi et al., 2017), tumorigenesis (Xu et al., 2015), and ischemic injury (Pandi et al., 2013). However, whether the downregulation of *Dnmt3a* following the critical period of CH methylation during postnatal brain maturation is regulated by miRNAs is unknown.

Here, we conducted an unbiased screen to identify miRNAs that are specifically induced during postnatal brain maturation. We found all three members of the miR-29 family to be highly induced during this period. Conditional deletion of all three miR-29 members in the brain resulted in the dysregulation of DNMT3a and CH hypermethylation that was associated with severe neurological dysfunction and premature lethality. Using a novel *Dnmt3a* mouse model, we then precisely assessed the direct consequences of disrupting the targeting of *Dnmt3a* by miR-29 *in vivo*. Our results identify miR-29 as an essential regulator of CH methylation via its targeting of *Dnmt3a* and define the importance of restricting CH methylation to a critical period during brain maturation.

RESULTS

miR-29 is the most upregulated miRNA during postnatal brain development

To screen for miRNAs that are induced during brain maturation, we examined the mouse cerebellum, because the timeline for cerebellar postnatal development is well defined. Cerebellar granule neuron precursors undergo rapid proliferation and complete their differentiation into cerebellar granule neurons by postnatal day 18 (P18) (Hatten and Roussel, 2011). Thus, we probed for miRNAs that are differentially expressed between young (P18) and adult (P250) cerebellum. We found that the most upregulated miRNAs in the adult belonged to the miRNA-29 (miR-29) family, which

were strikingly increased ~50- to 70-fold (Figure 1A; Table S1). The miR-29 family consists of three members—miR-29a, miR-29b, and miR-29c—that are expressed from two genomic loci: miR-29ab1 and miR-29b2c (Kriegel et al., 2012). Quantitative PCR analysis for miR-29b, which is expressed from both loci, confirmed that miR-29 expression was markedly increased during late cerebellar maturation (Figure 1B). This increase in miR-29b expression is even more evident in the cortex where the expression of miR-29 is very low during the embryonic period (between E13.5 and P0) but increases substantially postnatally (Li et al., 2014) (starting at P7, Figure 1C). Importantly, although miR-29b shows the highest fold induction, all three miR-29 family members were markedly induced during postnatal cortical maturation (Figures 1D–1F), as seen in the cerebellum (Figure 1A).

miR-29 expression in the brain is essential for normal postnatal development

To examine whether miR-29 is functionally important during brain maturation *in vivo*, we generated mice that were floxed for both alleles of miR-29. Specifically, miR-29ab1^{fl/fl} and miR-29b2c^{fl/fl} mice were crossed together such that all three members of the miR-29 family could be deleted in the presence of a Cre recombinase. Mice deleted for miR-29, either globally (with CMV-Cre-expressing mice; miR-29^{CMV}) or selectively in the brain (with Nestin-Cre-expressing mice; miR-29^{Nestin}), were born at the expected Mendelian ratio, appeared normal at birth, and were indistinguishable from wild-type (WT) littermate controls at postnatal day 10. However, starting at 10 days, the miR-29 knockouts began to exhibit retarded growth, with all mice dying by 45 days of age (Figures 1G–1J and S1A–S1D). Partial deletion of miR-29 from either locus also resulted in lethality by 150 days (Figure S1E). Importantly, consistent with the finding that miR-29 is not expressed during the stages of early brain development, complete deletion of miR-29 in either the miR-29^{CMV} or miR-29^{Nestin} mouse brains did not result in noticeable apoptosis or gross developmental brain malformations at P30 (Figures S1F and S1G).

Deletion of miR-29 in the brain elicits severe neurobehavioral abnormalities

Partial inactivation of miR-29ab1 was previously shown to result in motor dysfunction (Papadopoulou et al., 2015; Roshan et al., 2014). Thus, we examined the behavioral deficits of brain-selective miR-29-deleted mice (P30–P40). Loss of miR-29 in the brain led to ataxic movements and motor deficits, including hindlimb claspings as well as deficits in wire hanging and rotarod tests (Figures 2A, 2B, S2A, and S2B). These mice also demonstrated many features seen in mouse models of neurodevelopmental disorders. For example, the miR-29^{Nestin} mice exhibited repetitive, excessive self-grooming behavior by 20 days of age that led to facial hair loss and self-inflicted ulcerative skin lesions (Figures 2C and 2D; Video S1). Additionally, these mice were hyperactive in open field analyses with an increase in the total distance traveled as well as greater fine movements, a measure of stereotypic behavior (Figures 2E and S2C). miR-29^{Nestin} mice also spent significantly more time in the center region of the open field, suggesting a loss of cautionary avoidance of a novel open area (Figure 2F). The miR-29^{Nestin} mice displayed impaired sensorimotor

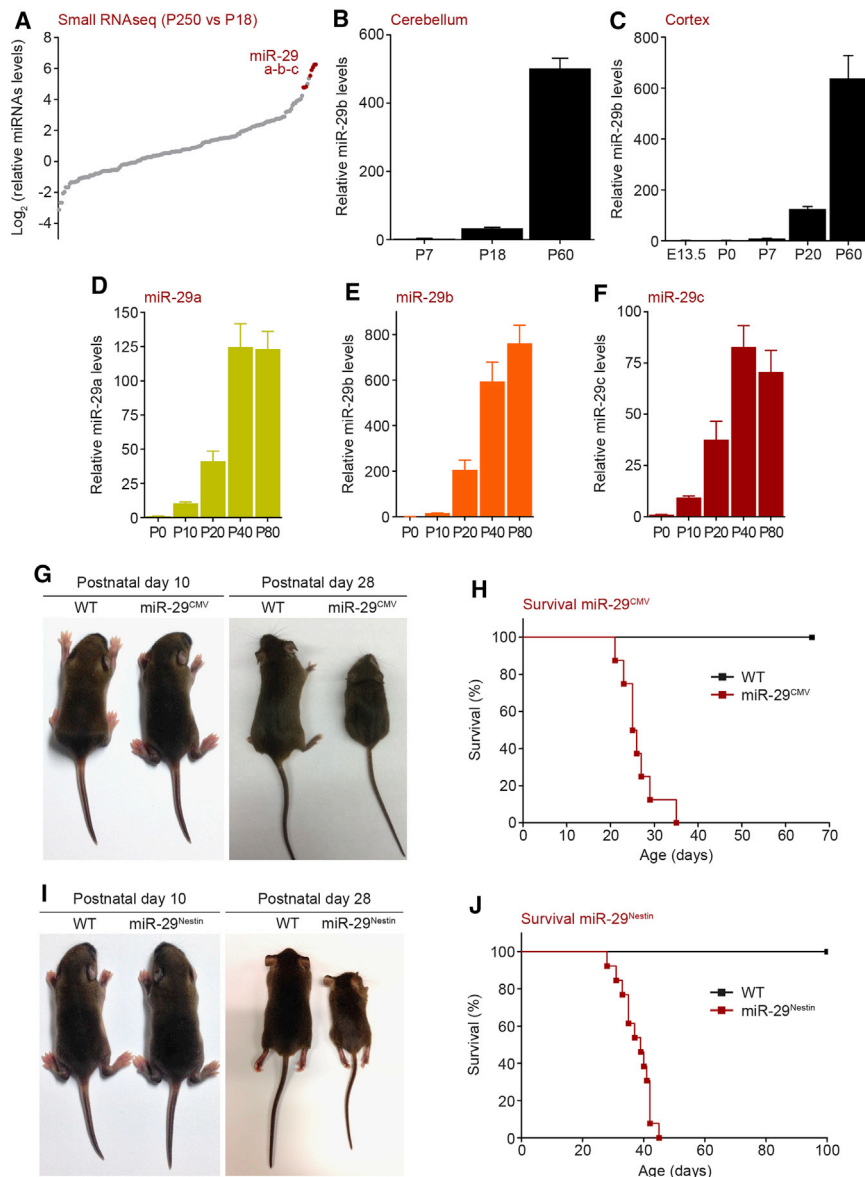


Figure 1. miR-29 is sharply upregulated during postnatal brain maturation and is essential for normal postnatal development

(A) Small RNA sequencing of postnatal P250 versus P18 WT mouse cerebellum. (B) Quantitative PCR (normalized to U6) analysis of miR-29b levels in the developing WT mouse cerebellum (n = 3). Fold change of miRNA levels compared to P7 are represented. (C) Quantitative PCR (normalized to U6) analysis of miR-29b levels in the developing WT mouse cortex (n = 3). Fold change of miRNA levels compared to E13.5 are represented. (D–F) Quantitative PCR (normalized to U6) analysis of miR-29a (D), miR-29b (E), and miR-29c (F) levels in the developing WT mouse cortex (n = 4). Fold change of miRNA levels compared to P0 are represented. (G) Pictures of WT (left) and miR-29ab1^{ff}, miR-29b2c^{ff}, CMV-Cre (miR-29^{CMV}) knockout mice (right) at postnatal P10 and P28. (H) Kaplan-Meier survival curve of miR-29^{CMV} knockout mice (WT, miR-29^{CMV} n = 8; miR-29^{CMV} median survival: 25.5 days). (I) Pictures of WT (left) and miR-29ab1^{ff}, miR-29b2c^{ff}, Nestin-Cre (miR-29^{Nestin}) knockout mice (right) at postnatal P10 and P28. (J) Kaplan-Meier survival curve of miR-29^{Nestin} knockout mice (WT n = 12; miR-29^{Nestin} n = 13; miR-29^{Nestin} median survival: 39 days). Means ± SEM are shown, value n represents the number of independent animals used. See also Figure S1 and Table S1.

gating in an acoustic startle test (Figure S2D). Importantly, we observed spontaneous seizures in a subset of these mice that subsequently led to their death. Thus, we examined whether miR-29-deficient mice were more susceptible to kainic acid-induced seizures. All miR-29^{Nestin} mice underwent tonic-clonic seizures and died within 25 min after kainic acid injection, while none of the WT mice sustained seizures or died with the same dose of kainic acid (Figures 2G, 2H, and S2E). Together, these findings show that loss of miR-29 leads to numerous neurobehavioral abnormalities, including an increased risk of seizures.

miR-29 deficiency results in the downregulation of many neuronal genes

To gain insight into the specific pathways affected in the miR-29-deficient mice, we conducted an RNA sequencing (RNA-seq)

analysis of WT and miR-29^{Nestin} cortices and found 2,823 annotated genes to be differentially expressed (false discovery rate [FDR] <0.1) (Figure 3A; Table S2). As expected from the knockout of a miRNA, many genes were upregulated. Indeed, an unbiased query identified miR-29 as the miRNA predicted to target the largest number of upregulated genes in this gene set (e.g., of the 1,346 upregulated genes, 245 genes are predicted direct targets of miR-29) (Figure 3B; Table S2). Rather unexpectedly, however, miR-29 deletion also resulted in the downregulation of a similarly large number of genes (1,477 genes downregulated) (Figure 3A; Table S2). Importantly, a pathway analysis revealed that, unlike the upregulated genes, the downregulated genes were most significantly associated with many neuronal functions, including axon guidance and synaptic transmission (Figures 3C, 3D, and S3A; Table S2). This set of downregulated genes is also associated with a variety of neuropsychiatric disorders such as autism, schizophrenia, and epilepsy, consistent with the observed behavioral deficits (Figures 3E and S3B; Table S2). These results suggest that the genes downregulated in the miR-29-deficient brains, which are unlikely to be direct targets of miR-29, are associated with the neurological dysfunction observed in the miR-29^{Nestin} mice.

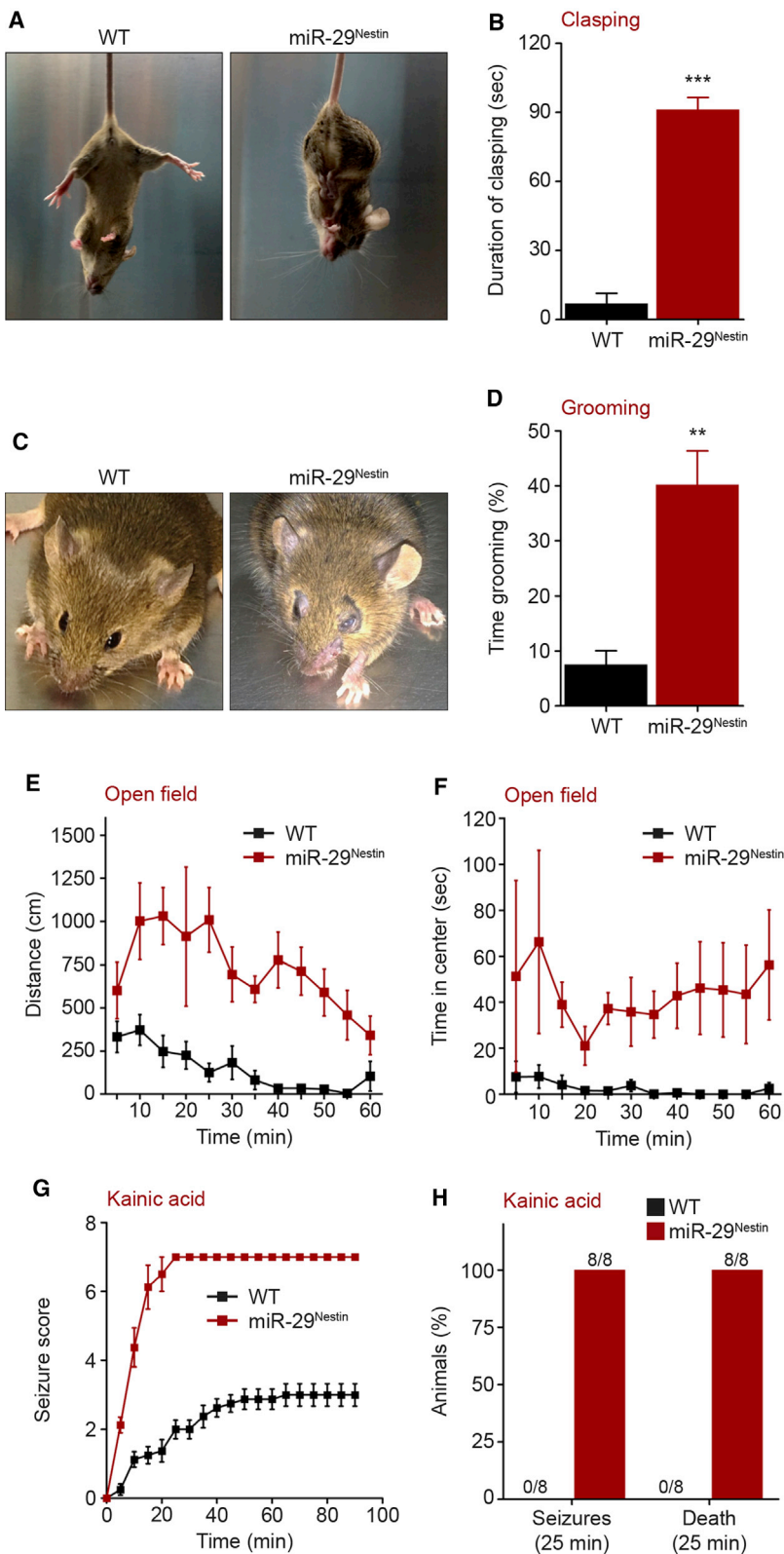


Figure 2. miR-29 deficiency in the brain results in neurological deficits and susceptibility to seizures

(A and B) Pictures (A) and quantification (B) of hindlimb claspings duration upon tail suspension (90 s) of WT and miR-29^{Nestlin} knockout mice (WT, miR-29^{Nestlin} n = 4; unpaired, two-tailed Student's t test ***p < 0.0001). (C and D) Pictures of facial lesions (C) and time spent grooming (D) over 30-min test (WT n = 4, miR-29^{Nestlin} n = 3; unpaired, two-tailed Student's t test **p = 0.0028). (E and F) Total distance traveled (E) and time spent in the center (F) of an open field chamber (60-min trial) (WT, miR-29^{Nestlin} n = 7; repeated-measures ANOVA, [E] total distance traveled: genotype effect F[1,12] = 52.28, ***p < 0.0001; [F] time spent in the center: genotype effect F [1,12] = 10.51, **p = 0.0071). (G) Seizure score following intraperitoneal injection of kainic acid (30 mg/kg). The behavioral scores were 1: hypoactivity; 2: head nodding; 3: anterior clonus; 4: loss of balance or repeated falling; 5: severe tonic-clonic seizures; 6: jumping; and 7: death (WT, miR-29^{Nestlin} n = 8; two-tailed nonparametric Mann-Whitney test: ***p < 0.0001). (H) Quantification of seizures and death 25 min after intraperitoneal injection of kainic acid (30 mg/kg) (WT, miR-29^{Nestlin} n = 8). Behaviors and seizures were analyzed at P30–P40. Means ± SEM are shown, value n represents the number of independent animals used, **p = 0.01–0.001, ***p < 0.001. See also [Figure S2](#) and [Video S1](#).

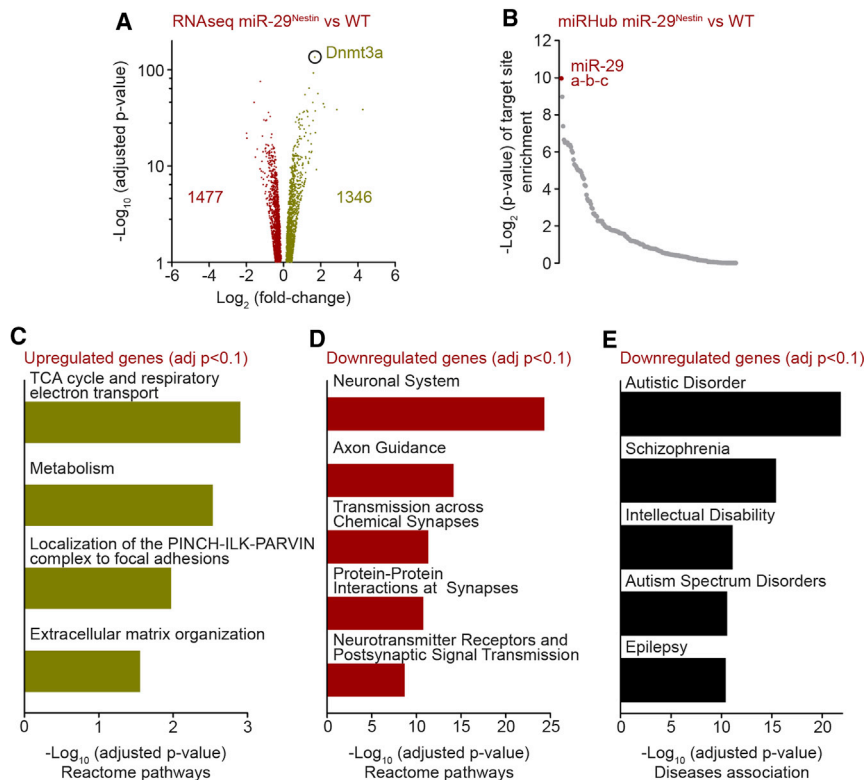


Figure 3. Downregulated genes are involved in neuronal functions in miR-29-deficient brains

(A) Volcano plot of differentially expressed genes (DESeq2 adjusted p value [adj.p] <0.1) obtained from RNA-seq analysis of P40 WT and miR-29^{Nestin} mice cortex (WT, miR-29^{Nestin} n = 3). Value n represents the number of independent animals used. (B) MiRHub analysis of upregulated genes in miR-29^{Nestin} cortex compared to WT cortex. The targeting score for each miRNA was normalized to the 3' UTR length of the genes of interest. (C and D) Reactome pathway (top terms) analysis of differentially expressed genes in miR-29^{Nestin} cortex. (E) DisGeNET disease association (top terms) analysis of downregulated genes in miR-29^{Nestin} cortex. See also Figure S3 and Table S2.

miR-29-deficient brains have increased DNMT3A expression and CH hypermethylation of neuronal genes

To determine how miR-29 deficiency could result in reduced neuronal gene expression, we examined whether any of the direct targets of miR-29 could modulate gene transcription. Among the top ten upregulated genes in the miR-29-deficient brains was the DNA methyltransferase *Dnmt3a* (Table S2), which can epigenetically regulate gene expression. *Dnmt3a* expression is known to be tightly regulated in the postnatal brain where it is induced at birth and then sharply declines several weeks later (Feng et al., 2005; Lister et al., 2013). However, the mechanisms that repress DNMT3A expression have not yet been identified. Interestingly, the marked increase in miR-29 starting at P20 coincides with the selective and sharp decrease in *Dnmt3a* expression that occurs during this period (Figures S4A–S4C) (Feng et al., 2005; Lister et al., 2013). *Dnmt3a* is known to have multiple evolutionarily conserved miR-29-binding sites in its 3' UTR (Figure S4D) and has been shown to be targeted by miR-29 (Fabbri et al., 2007; Pandi et al., 2013; Xu et al., 2015). Consistent with the upregulation of *Dnmt3a* detected by RNA-seq in miR-29^{Nestin} cortex, we found the DNMT3A protein to be markedly elevated in multiple brain regions of the miR-29-deficient mice at P40, a stage at which WT brains have already reduced DNMT3A (Figures 4A–4D).

DNMT3a is particularly relevant in the context of brain maturation, because it plays an essential role in *de novo* methylation of the neuronal genome at non-canonical (non-CG) sites

WT and miR-29^{Nestin} mice revealed that, although there was no increase in CG methylation, loss of miR-29 in the brain led to a striking increase in CH methylation within gene regions (Figure 4E; Table S3). The most prominent increase was observed at CA and CT sites and, to a lesser extent, at CC sites (Figures S4E–S4G).

Although hypermethylation is generally believed to result in gene downregulation (Luo et al., 2016; Moore et al., 2013), recent studies point to a more complex relationship between gene methylation and expression (Keown et al., 2017; Lavery and Zoghbi, 2019; Rizzardi et al., 2019). In our model, although both the upregulated and downregulated genes were CH hypermethylated upon loss of miR-29 expression, there was a small but significant increase in CH hypermethylation in the downregulated genes compared to upregulated genes in the miR-29^{Nestin} cortex (Figure 4F).

Mice with selective disruption of miR-29 binding to *Dnmt3a* 3' UTR have neurological deficits

Our results with the miR-29-deleted mice underscore the importance of miR-29 in brain maturation and, specifically, its function in restricting the critical period of CH methylation in the maturing brain potentially via its ability to target *Dnmt3a*. However, in addition to *Dnmt3a*, miR-29 has multiple gene targets, several of which are also upregulated in the brains of miR-29-deleted mice (Table S2). To identify the consequences of disrupting the ability of miR-29 to target *only Dnmt3a*, we developed a novel knockin mouse model in which five binding sites of miR-29 in

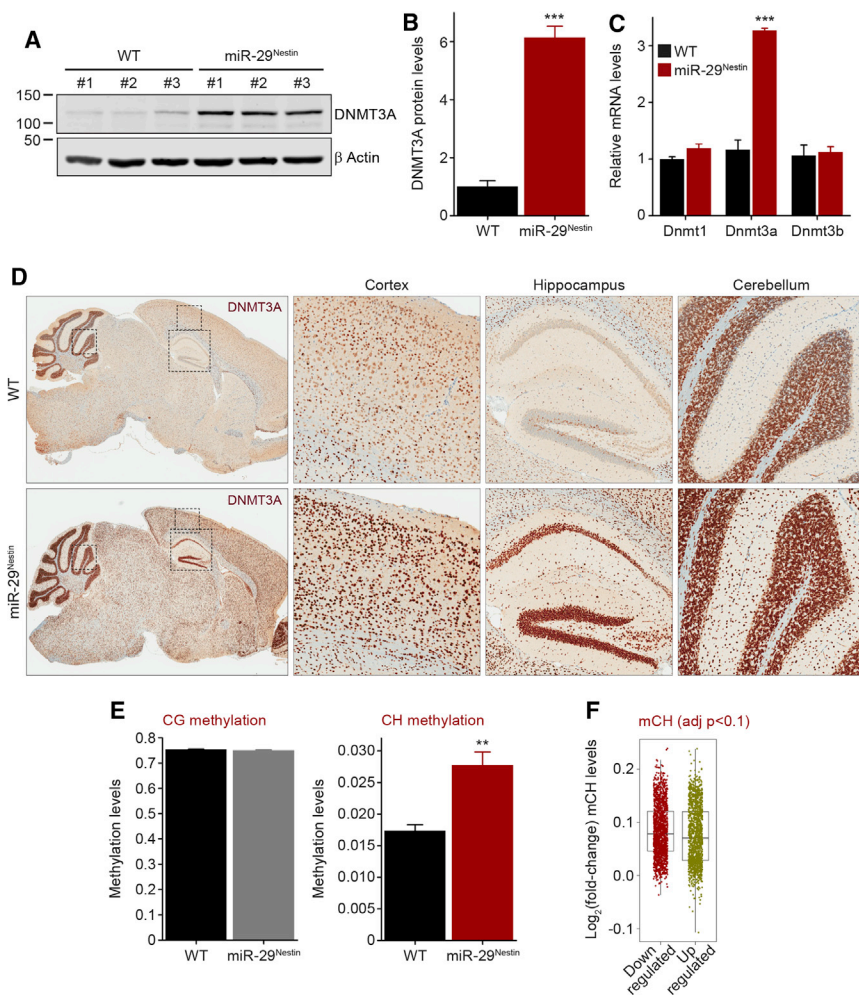


Figure 4. DNMT3A levels and CH methylation are increased in miR-29-deficient brains

(A and B) Western blot analysis of DNMT3A protein levels in three P40 WT and miR-29^{Nestin} cortices (WT, miR-29^{Nestin} n = 3). Quantifications were normalized to β actin levels (B) (unpaired, two-tailed Student's t test ***p = 0.0003).

(C) Comparison of *Dnmt1*, *Dnmt3a*, and *Dnmt3b* mRNA levels, normalized to *Gapdh*, by qPCR in P40 WT and miR-29^{Nestin} brains (WT, miR-29^{Nestin} n = 3; multiple unpaired t test with Holm-Sidak correction, *Dnmt3a*: ***p < 0.0001).

(D) Representative images of WT and miR-29^{Nestin} mouse (P40) brains immunostained for DNMT3A. Enlargement of cortical, hippocampal, and cerebellar regions are shown.

(E) CG and non-CG (CH) methylation within gene regions quantified by bisulfite sequencing of genomic DNA extracted from the cortex of P40 WT and miR-29^{Nestin} mice (WT, miR-29^{Nestin} n = 4; unpaired, two-tailed Student's t test, CH: **p = 0.0039).

(F) Fold-change of CH methylation levels in down-regulated (red) and upregulated (green) gene regions of miR-29^{Nestin} cortex compared to WT cortex (WT, miR-29^{Nestin} n = 3; Welch's t test p = 1.567e-05). Means \pm SEM are shown except in (F): medians \pm 1.5 interquartile range (IQR) are shown. Value n represents the number of independent animals used, **p = 0.01-0.001, ***p < 0.001. See also Figure S4 and Table S3.

Dnmt3a^{mi5} mice exhibit downregulation and CH hypermethylation of genes associated with neurodevelopmental disorders

To confirm that the *Dnmt3a*^{mi5} mice had increased DNMT3A activity, we quantified CH methylation in the cortex of WT and *Dnmt3a*^{mi5} mice. As observed with miR-

29^{Nestin} mice, there was no difference in CG methylation, but a marked increase in CH methylation within genes in *Dnmt3a*^{mi5} mice (Figures 6A and S6A-S6C; Table S4). To examine the consequences of CH hypermethylation, we conducted an RNA-seq analysis of cortical samples from WT and *Dnmt3a*^{mi5} mice. As expected from a mouse model designed for miR-29 to selectively target *Dnmt3a*, fewer differentially expressed genes (109 downregulated and 34 upregulated genes, FDR <0.1) were observed in the *Dnmt3a*^{mi5} compared to the miR-29^{Nestin} cortex (Figure 6B; Table S5). However, it is interesting to note that the *Dnmt3a*^{mi5} cortex had disproportionately more downregulated genes. These downregulated genes exhibited a significant increase in CH methylation as compared to the upregulated genes, a feature that was also seen in the miR-29^{Nestin} cortex (Figure 6C). A pathway analysis revealed that many of the genes that were downregulated in the cortex of *Dnmt3a*^{mi5} mice were associated with neuronal functions or signaling (Figure 6D; Table S5). Interestingly, as seen in the miR-29^{Nestin} cortex, these genes were also associated with neurodevelopmental disorders including mental retardation, bipolar disorder, schizophrenia, epilepsy, and ASD (Figure 6E; Table S5).

the 3' UTR region of *Dnmt3a* were mutated (hereafter referred to as *Dnmt3a*^{mi5} mice) (Figure 5A). In these mice, miR-29 should still be able to inhibit all of its target genes except *Dnmt3a*. Consistent with our expectation that miR-29 directly restricts *Dnmt3a* expression during brain maturation, we found that *Dnmt3a*^{mi5} mice selectively express higher levels of DNMT3A (Figures 5B-5D). *Dnmt3a*^{mi5} mice were born at the expected Mendelian ratio and appeared indistinguishable from WT controls at birth and during the early postnatal period. However, *Dnmt3a*^{mi5} mice had a reduced lifespan, albeit at a later time point compared to the miR-29^{Nestin} mice (median survival of 14 months) (Figure 5E). The *Dnmt3a*^{mi5} mice at these late stages displayed severe dermatitis, which did not appear to be due to excessive grooming (Figures S5A and S5B). Although *Dnmt3a*^{mi5} mice seem normal at P40, they begin exhibiting hindlimb clasp at ~1 year of age (Figures 5F and 5G). Interestingly, during this 1 year time frame, although these mice did not exhibit overt hyperactivity, they showed increased susceptibility to kainic acid-induced seizures and death as seen in the miR-29^{Nestin} mice (Figures 5H, 5I, and S5C).

29^{Nestin} mice, there was no difference in CG methylation, but a marked increase in CH methylation within genes in *Dnmt3a*^{mi5} mice (Figures 6A and S6A-S6C; Table S4). To examine the consequences of CH hypermethylation, we conducted an RNA-seq analysis of cortical samples from WT and *Dnmt3a*^{mi5} mice. As expected from a mouse model designed for miR-29 to selectively target *Dnmt3a*, fewer differentially expressed genes (109 downregulated and 34 upregulated genes, FDR <0.1) were observed in the *Dnmt3a*^{mi5} compared to the miR-29^{Nestin} cortex (Figure 6B; Table S5). However, it is interesting to note that the *Dnmt3a*^{mi5} cortex had disproportionately more downregulated genes. These downregulated genes exhibited a significant increase in CH methylation as compared to the upregulated genes, a feature that was also seen in the miR-29^{Nestin} cortex (Figure 6C). A pathway analysis revealed that many of the genes that were downregulated in the cortex of *Dnmt3a*^{mi5} mice were associated with neuronal functions or signaling (Figure 6D; Table S5). Interestingly, as seen in the miR-29^{Nestin} cortex, these genes were also associated with neurodevelopmental disorders including mental retardation, bipolar disorder, schizophrenia, epilepsy, and ASD (Figure 6E; Table S5).

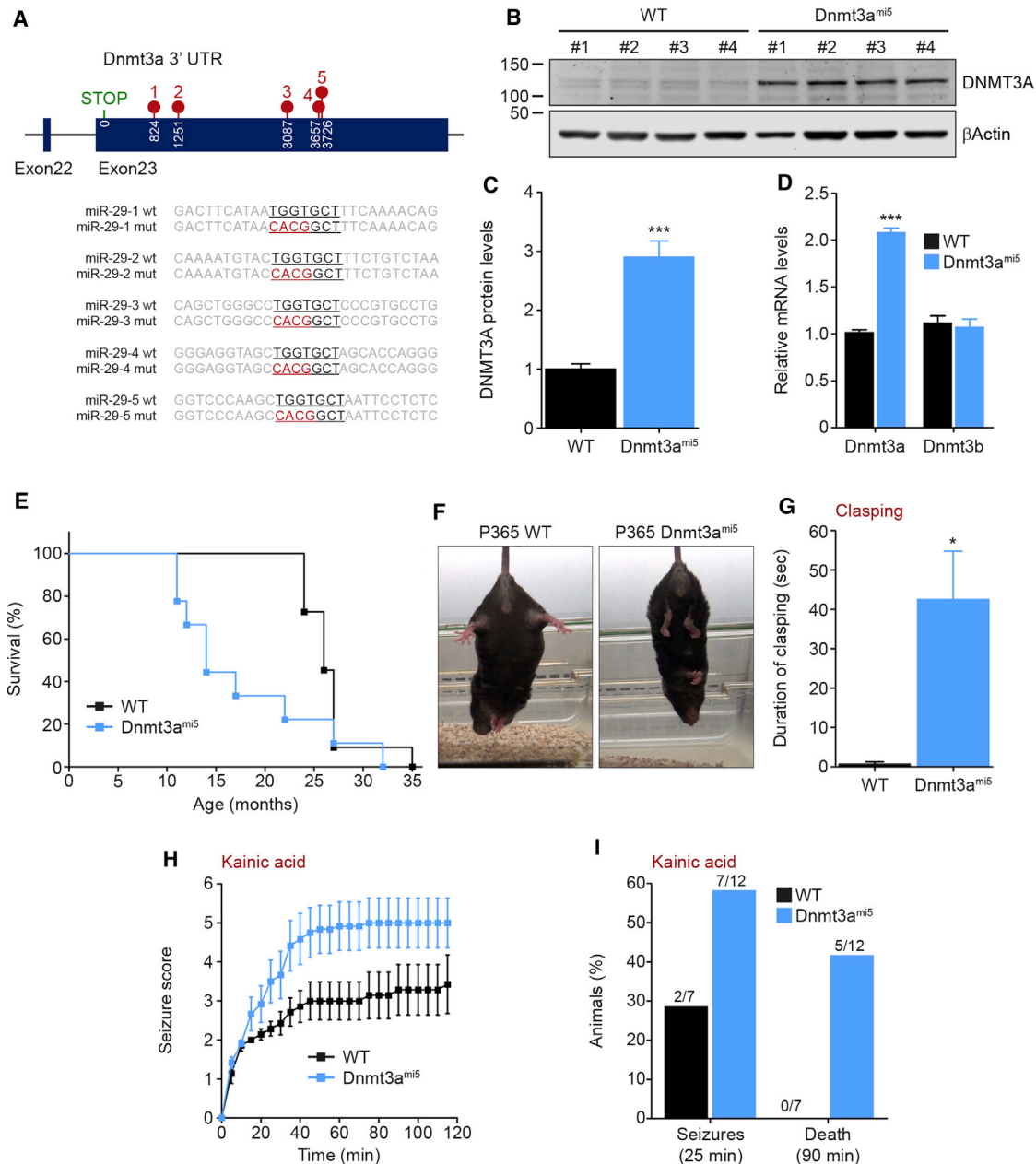


Figure 5. Mice unable to restrict *Dnmt3a* expression via miR-29 display neurological deficits and susceptibility to seizures

(A) Schematic representation of the CRISPR/Cas9 mutagenesis of five miR-29 binding sites in *Dnmt3a* 3'UTR performed to generate the *Dnmt3a*^{mi5} knock-in mice. (B and C) DNMT3A protein levels analyzed by western blot in three 4.5-month-old WT and *Dnmt3a*^{mi5} cortices (WT, *Dnmt3a*^{mi5} n = 4). Quantification were normalized to β actin levels (C) (unpaired, two-tailed Student's t test, ***p = 0.0004). (D) *Dnmt3a* and *Dnmt3b* mRNA levels analyzed by qPCR in 4.5-month-old WT and *Dnmt3a*^{mi5} cortex. Quantification was normalized to *Gapdh* levels (WT, *Dnmt3a*^{mi5} n = 4; unpaired, two-tailed Student's t test, *Dnmt3a*: ***p < 0.0001). (E) Kaplan-Meier survival curve of *Dnmt3a*^{mi5} mice (WT n = 11, *Dnmt3a*^{mi5} n = 9; median survival: WT 26 months, *Dnmt3a*^{mi5} 14 months; Gehan-Breslow-Wilcoxon test, **p = 0.0086). (F and G) Pictures (F) and quantification (G) of hindlimb clasping upon suspension (60 s) of 1-year-old WT and *Dnmt3a*^{mi5} mice (WT n = 3, *Dnmt3a*^{mi5} n = 4, unpaired, two-tailed Student's t test *p = 0.0351). (H) Seizure score following intraperitoneal injection of kainic acid (30 mg/kg) to 4.5-month-old WT and *Dnmt3a*^{mi5} mice. The behavioral scores were 1: hypoactivity; 2: head nodding; 3: anterior clonus; 4: loss of balance or repeated falling; 5: severe tonic-clonic seizures; 6: jumping; and 7: death (WT n = 7, *Dnmt3a*^{mi5} n = 12; two-tailed nonparametric Mann-Whitney test: ***p < 0.0001). (I) Quantification of seizures (25 min) and death (90 min) after intraperitoneal injection of kainic acid (30 mg/kg), (WT n = 7, *Dnmt3a*^{mi5} n = 12). Means ± SEM are shown, value n represents the number of independent animals used, *p = 0.05–0.01, ***p < 0.001. See also Figure S5.

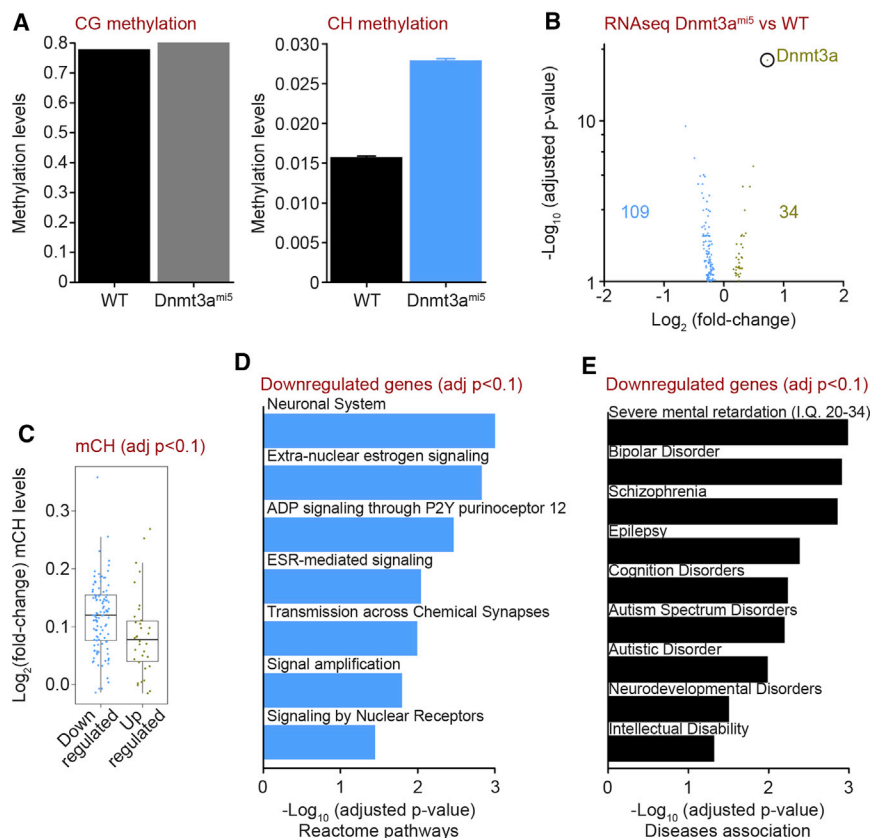


Figure 6. Mice unable to restrict *Dnmt3a* expression via miR-29 have downregulated genes involved in neuronal signaling and neurodevelopmental disorders.

(A) CG and CH methylation of gene regions quantified by bisulfite sequencing of genomic DNA extracted from the cortex of 4.5-month-old WT and Dnmt3a^{mi5} cortex (WT, Dnmt3a^{mi5} n = 2). Means ± SEM are shown.

(B) Volcano plot of differentially expressed genes (DESeq2 adj.p < 0.1) obtained from RNA-seq analysis of 4.5-month-old WT and Dnmt3a^{mi5} cortex (WT, Dnmt3a^{mi5} n = 4).

(C) Fold-change of CH methylation in downregulated (blue) and upregulated (green) gene regions of Dnmt3a^{mi5} cortex compared to WT cortex (WT, Dnmt3a^{mi5} n = 4; Welch's t test p = 0.01986). Medians ± 1.5 IQR are shown.

(D and E) Reactome pathway (D) and DisGeNET disease association analysis (E) of downregulated genes in Dnmt3a^{mi5} cortex.

Value n represents the number of independent animals used. See also Figure S6 and Tables S4 and S5.

DISCUSSION

Our results highlight the induction of miR-29 as an event that is crucial for multiple aspects of brain maturation. We found that miR-29, which is induced several hundred fold in the postnatal brain, was not essential for embryonic brain devel-

miR-29 controls a set of genes associated with neuronal activity via DNMT3A in the brain

The miR-29^{Nestin} mice exhibited a complex phenotype associated with the aberrant expression of a large set of genes, some of which were unexpectedly downregulated. In order to identify the specific role played by DNMT3A in this phenotype, we compared the genes differentially expressed in the cortex of miR-29^{Nestin} mice with those deregulated in the cortex of Dnmt3a^{mi5} mice. Among the differentially expressed genes in the Dnmt3a^{mi5} cortex, there was a substantial overlap between the downregulated genes in Dnmt3a^{mi5} and miR-29^{Nestin} cortex (Figure 7A). The 55 commonly downregulated genes also exhibited a strong correlation in CH methylation levels between both models (Figure 7B). Interestingly, many of these genes have important neuronal functions including *Gabrb3* (GABA receptor), *Kcnv1* (K⁺ channel), *Nlgn1* (Neuroigin 1), and *Nrxn1* (Neurexin 1) (Figure 7C). A pathway analysis showed that the commonly downregulated genes are associated with neuronal functions, including neurotransmission and synaptic signaling (Figure 7D; Table S6). Importantly, these downregulated genes are also associated with many neuropsychiatric disorders such as autism, epilepsy, and schizophrenia (Figure 7E; Table S6). Thus, the loss of miR-29 and the selective inability of miR-29 to target *Dnmt3a* resulted in the CH hypermethylation and downregulation of a critical set of neuronal genes that are important for establishing normal brain homeostasis.

opment but was crucial for postnatal brain maturation and homeostasis. Failure to express miR-29 resulted in severe consequences, including hyperactive behaviors, susceptibility to seizures, and premature lethality. Consistent with our observations, dysregulation of miR-29 is associated with psychiatric disorders such as schizophrenia and bipolar disorder (Geaghan and Cairns, 2015; Tonacci et al., 2019). Additionally, reduced expression of miR-29 is observed in multiple contexts of brain dysfunction including ischemia (Khanna et al., 2013; Pandi et al., 2013) and neurodegenerative disorders such as Alzheimer's (Hébert et al., 2008; Lei et al., 2015) and Parkinson's disease (Bai et al., 2017; Margis et al., 2011). Interestingly, reducing the levels of miR-29 in neurons of the turquoise killifish resulted in metabolic stress and aging (Ripa et al., 2017). Together, these results indicate that high levels of miR-29 in the postnatal brain are essential for the maintenance of healthy brain function.

The exact mechanisms that regulate the expression of the miR-29 family genes in the brain either during normal development or in neurodevelopmental disorders are unclear. Although all three miR-29 family genes are induced during brain maturation, our observation that miR-29b is disproportionately upregulated suggests that mechanisms controlling miRNA biogenesis (e.g., processing, stability), in addition to transcriptional upregulation, are likely implicated. For example, changes in miRNA biogenesis machinery (*DGCR8* and *DICER1*) are thought to result in altered miRNA expression in the brains of patients

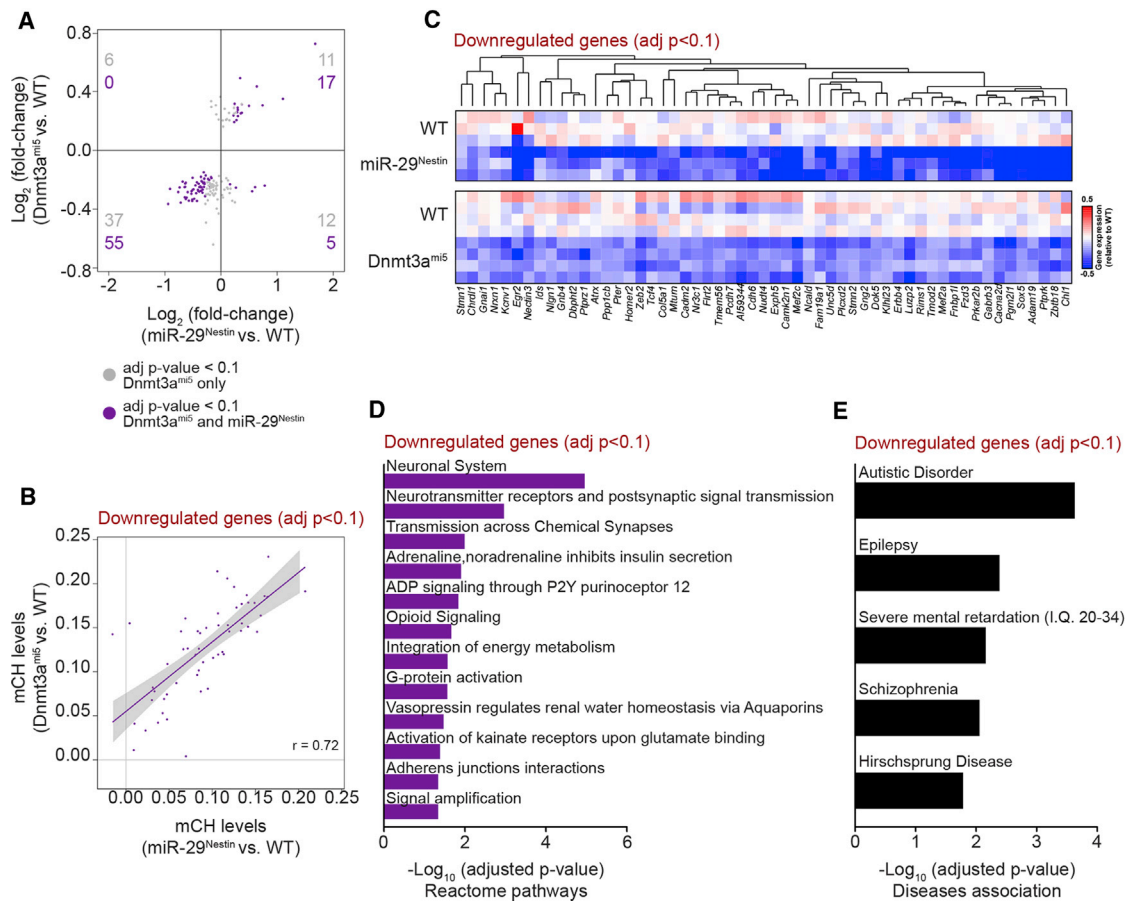


Figure 7. Cortex from miR-29^{Nestin} and Dnmt3a^{mi5} mice have common downregulated genes involved in neuronal signaling, synaptic activity, and neuropsychiatric disorders

(A) Concordance of gene expression fold-changes between miR-29^{Nestin} cortex and Dnmt3a^{mi5} cortex (WT, miR-29^{Nestin} n = 3, WT, Dnmt3a^{mi5} n = 4). Among the genes that are differentially expressed (DESeq2 adj.p < 0.1) in 4.5-month-old Dnmt3a^{mi5} cortex, the genes also found differentially expressed (DESeq2 adj.p < 0.1) in miR-29^{Nestin} cortex (purple), and the genes uniquely differentially expressed in Dnmt3a^{mi5} cortex (gray) are shown.

(B) Concordance of CH methylation levels in genes commonly downregulated in miR-29^{Nestin} and Dnmt3a^{mi5} cortex (Pearson correlation $r = 0.72$).

(C–E) Heatmap (C), Reactome pathway analysis (D), and DisGeNET disease association analysis (E) of genes commonly downregulated in miR-29^{Nestin} and Dnmt3a^{mi5} cortex.

Value n represents the number of independent animals used. See also Table S6.

with schizophrenia (Beveridge et al., 2010; Santarelli et al., 2011), temporal lobe epilepsy (McKiernan et al., 2012), and in 22q11.2 microdeletion carriers (Stark et al., 2008). These observations are interesting, because DGCR8 and DICER1 appear to differentially affect the expression of the three miR-29 family members in postmitotic neurons (Babiarz et al., 2011).

Although brain maturation is recognized as a period during which experience can fine-tune neuronal activity, the epigenetic mechanisms by which this is achieved are just starting to become uncovered. A major clue has come from recent studies, which found that the early postnatal maturing brain undergoes non-canonical CH methylation mediated by DNMT3A during a critical period (Chen et al., 2015; Gabel et al., 2015; Guo et al., 2014; He and Ecker, 2015; Kinde et al., 2015; Lister et al., 2013; Mo et al., 2015; Xie et al., 2012). However, exactly how DNMT3A expression is regulated and the consequences of unrestricted CH methylation were unknown. Our results identify

miR-29 as a key regulator of CH methylation during brain maturation via its ability to target *Dnmt3a*. Mice in which miR-29 is either deleted or unable to target *Dnmt3a*, sustain elevated levels of DNMT3A in the mature brain, resulting in hypermethylation at CH sites. Although DNMT3A can mediate both CG and CH methylation, we did not observe any changes in levels of CG methylation at the gene regions or at CpG islands (data not shown) in these mice, a finding that is consistent with the observation that DNMT3A primarily mediates CH methylation during brain maturation.

Interestingly, CH hypermethylation occurred in both the downregulated and upregulated genes, although the levels of CH methylation were higher in the downregulated genes. These results indicate that, although CH methylation is an important factor in the downregulation of gene expression, it alone does not seem to be sufficient to predict whether a specific gene will be upregulated or downregulated. For example, downregulation

of some genes (e.g., those coding for a transcriptional repressor), may have secondary effects that increase the expression of their target genes despite their methylation status. Alternatively, some hypermethylated genomic regions may be more efficient at recruiting the gene repression machinery at the expense of other hypermethylated genomic regions, leading to different outcomes on gene expression.

CH methylated DNA is recognized by MeCP2, a protein that primarily functions to mediate transcriptional repression of neuronal genes. Consequently, genes that are methylated at CH sites during brain maturation are preferentially reduced with MeCP2 duplication (Chen et al., 2015; Gabel et al., 2015). Interestingly, mice overexpressing MeCP2 develop multiple neurological abnormalities that are also similar to the defects observed in our miR-29-deficient and Dnmt3a^{mi5} mice, including seizures, as well as premature death (Collins et al., 2004). The fact that both MeCP2-overexpressing mice and miR-29-deficient mice appear normal at birth but then progressively deteriorate illustrates the essential role that these molecules play selectively during brain maturation. Consistent with this, we observed a substantial overlap between the genes downregulated by removal of miR-29 and the gene upregulated in MeCP2 null mouse models (Figure S4H; Table S7). The relevance of regulating CH methylation and fine-tuning neuronal gene expression in humans is underscored by the fact that both the loss or duplication of MeCP2 result in Rett syndrome or intellectual disability, respectively (Lavery and Zoghbi, 2019; Lombardi et al., 2015).

The striking importance of miR-29 in brain maturation is emphasized by the fact that the miR-29-deficient mice exhibited complex behavioral phenotypes. This collection of phenotypes is likely due to the dysregulation of a large number of genes in the miR-29-deficient mice. The Dnmt3a^{mi5} mice that we generated have, however, allowed us to focus specifically on the consequences of CH hypermethylation that result from the inability of miR-29 to target *Dnmt3a* alone. Interestingly, the Dnmt3a^{mi5} mice have more downregulated than upregulated genes, and these genes have an important role in neuronal activity and are associated with many neurodevelopmental disorders. As anticipated, not all of the phenotypes observed in the miR-29^{Nestin} mice were seen in the Dnmt3a^{mi5} mice. However, the genes downregulated in both models are important for neurotransmission and synaptic signaling and associated with ASD, epilepsy, mental retardation, and schizophrenia. Interestingly, both mouse models have increased susceptibility to seizures, a condition that is frequently associated with these disorders (Frye et al., 2016; Hagerman et al., 2017; Hüfner et al., 2015). In contrast, the behavioral phenotypes selectively observed in the miR-29^{Nestin} mice, which also reflect brain maturation abnormalities, are likely a consequence of the gene dysregulations that are unique to these mice.

Together, these results identify an essential function of miR-29 in brain maturation through its ability to target multiple pathways. Specifically, we show that miR-29 is a key regulator of DNMT3A-mediated CH methylation during brain maturation, also highlighting the importance of restricting CH methylation during a critical window for sustaining normal functions in the mature brain.

STAR★METHODS

Detailed methods are provided in the online version of this paper and include the following:

- KEY RESOURCES TABLE
- RESOURCE AVAILABILITY
 - Lead contact
 - Materials availability
 - Data and code availability
- EXPERIMENTAL MODEL AND SUBJECT DETAILS
- METHOD DETAILS
 - Generation of knock-out and knock-in mice
 - Small RNA sequencing and analysis
 - RT-qPCR analysis
 - Mouse behavioral analysis: hindlimb clasping
 - Grooming
 - Open field test
 - Acoustic startle test
 - Wire-hang test for grip strength
 - Rotarod test
 - Kainic acid-induced seizures scoring
 - Western blotting
 - Whole genome bisulfite-sequencing
 - RNA sequencing and analysis
 - miRHub analysis
 - Immunohistochemistry staining
- QUANTIFICATION AND STATISTICAL ANALYSIS

SUPPLEMENTAL INFORMATION

Supplemental information can be found online at <https://doi.org/10.1016/j.celrep.2021.108946>.

ACKNOWLEDGMENTS

We thank the members of the Deshmukh Lab for critical review of this manuscript. We also acknowledge Dr. Natalia Riddick, Viktoriya Nikolova, and Dr. Kara Agster at the UNC Mouse Behavioral Phenotyping Laboratory, for their technical assistance. We thank Mervi Eeva, Ying Li, and Bentley Midkiff at the UNC Translational Pathology Laboratory for expert technical assistance. We also appreciate the technical assistance provided by Janice Weaver and Carolyn Suitt at the UNC Animal Histopathology and the Center for Gastrointestinal Biology and Disease (CGIBD), respectively. The graphical abstract was created partly with [BioRender.com](https://www.biorender.com). This work was supported by NIH, United States (GM118331 and AG055304 to M.D.). H.S. is a Howard Hughes Medical Institute Fellow of the Damon Runyon Cancer Research Foundation, United States (DRG-2194-14). J.M.S. and T.S.P. were supported by The Eunice Kennedy Shriver National Institute of Child Health and Human Development (U54HD079124) and NINDS (P30NS045892) of United States. The UNC Mouse Behavioral Phenotyping Laboratory is supported by a grant from the National Institute of Child Health and Human Development (NICHD), United States (U54-HD079124). The UNC Translational Pathology Laboratory is supported in part by grants from the NCI (5P30CA016086-42), NIH (U54-CA156733), NIEHS (5 P30 ES010126-17), UCRF, and NCBT (2015-IDG-1007) of United States.

AUTHOR CONTRIBUTIONS

V.S., A.N., and E.H. conducted most of the experiments with help as described here. H.S. and M.E.G. performed the whole-genome bisulfite sequencing and its analyses. J.M.S. and T.S.P. analyzed all RNA-seq data. C.L.K., M.K., P.S.,

and S.M.H. performed small RNA-seq and miRHub analysis. C.P., J.G., and E.A. helped with imaging and analysis of immunohistochemical stains. C.F. and M.B. helped manage the mouse colony. J.L. and Y.-W.H. generated the miR-29-floxed mice. S.M. conducted and analyzed many of the neurobehavioral assessments. V.S., M.E.G., and M.D. outlined the project. M.D. supervised the project. V.S., A.N., E.H., and M.D. produced the final version of the manuscript.

DECLARATION OF INTERESTS

The authors declare no competing interests.

Received: July 28, 2020

Revised: December 9, 2020

Accepted: March 14, 2021

Published: April 6, 2021

REFERENCES

- Abe, M., and Bonini, N.M. (2013). MicroRNAs and neurodegeneration: role and impact. *Trends Cell Biol.* *23*, 30–36.
- Babiarz, J.E., Hsu, R., Melton, C., Thomas, M., Ullian, E.M., and Blelloch, R. (2011). A role for noncanonical microRNAs in the mammalian brain revealed by phenotypic differences in Dgcr8 versus Dicer1 knockouts and small RNA sequencing. *RNA* *17*, 1489–1501.
- Bai, X., Tang, Y., Yu, M., Wu, L., Liu, F., Ni, J., Wang, Z., Wang, J., Fei, J., Wang, W., et al. (2017). Downregulation of blood serum microRNA 29 family in patients with Parkinson's disease. *Sci. Rep.* *7*, 5411.
- Baran-Gale, J., Fannin, E.E., Kurtz, C.L., and Sethupathy, P. (2013). Beta cell 5'-shifted isomiRs are candidate regulatory hubs in type 2 diabetes. *PLoS ONE* *8*, e73240.
- Beveridge, N.J., Gardiner, E., Carroll, A.P., Tooney, P.A., and Cairns, M.J. (2010). Schizophrenia is associated with an increase in cortical microRNA biogenesis. *Mol. Psychiatry* *15*, 1176–1189.
- Biggar, K.K., Wu, C.-W., and Storey, K.B. (2014). High-throughput amplification of mature microRNAs in uncharacterized animal models using polyadenylated RNA and stem-loop reverse transcription polymerase chain reaction. *Anal. Biochem.* *462*, 32–34.
- Bourgeron, T. (2015). From the genetic architecture to synaptic plasticity in autism spectrum disorder. *Nat. Rev. Neurosci.* *16*, 551–563.
- Chahrour, M., Jung, S.Y., Shaw, C., Zhou, X., Wong, S.T., Qin, J., and Zoghbi, H.Y. (2008). MeCP2, a key contributor to neurological disease, activates and represses transcription. *Science* *320*, 1224–1229.
- Chen, L., Chen, K., Lavery, L.A., Baker, S.A., Shaw, C.A., Li, W., and Zoghbi, H.Y. (2015). MeCP2 binds to non-CG methylated DNA as neurons mature, influencing transcription and the timing of onset for Rett syndrome. *Proc. Natl. Acad. Sci. USA* *112*, 5509–5514.
- Collins, A.L., Levenson, J.M., Vilaythong, A.P., Richman, R., Armstrong, D.L., Noebels, J.L., David Sweatt, J., and Zoghbi, H.Y. (2004). Mild overexpression of MeCP2 causes a progressive neurological disorder in mice. *Hum. Mol. Genet.* *13*, 2679–2689.
- Dobin, A., Davis, C.A., Schlesinger, F., Drenkow, J., Zaleski, C., Jha, S., Batut, P., Chaisson, M., and Gingeras, T.R. (2013). STAR: ultrafast universal RNA-seq aligner. *Bioinformatics* *29*, 15–21.
- Dubes, S., Favereaux, A., Thoumine, O., and Letellier, M. (2019). miRNA-Dependent Control of Homeostatic Plasticity in Neurons. *Front. Cell. Neurosci.* *13*, 536. <https://doi.org/10.3389/fncel.2019.00536>.
- Edbauer, D., Neilson, J.R., Foster, K.A., Wang, C.-F., Seeburg, D.P., Batterton, M.N., Tada, T., Dolan, B.M., Sharp, P.A., and Sheng, M. (2010). Regulation of synaptic structure and function by FMRP-associated microRNAs miR-125b and miR-132. *Neuron* *65*, 373–384.
- Fabbri, M., Garzon, R., Cimmino, A., Liu, Z., Zanesi, N., Callegari, E., Liu, S., Alder, H., Costinean, S., Fernandez-Cymering, C., et al. (2007). MicroRNA-29 family reverts aberrant methylation in lung cancer by targeting DNA methyltransferases 3A and 3B. *Proc. Natl. Acad. Sci. USA* *104*, 15805–15810.
- Fabregat, A., Jupe, S., Matthews, L., Sidiropoulos, K., Gillespie, M., Garapati, P., Haw, R., Jassal, B., Korninger, F., May, B., et al. (2018). The Reactome Pathway Knowledgebase. *Nucleic Acids Res.* *46* (D1), D649–D655.
- Feng, J., Chang, H., Li, E., and Fan, G. (2005). Dynamic expression of de novo DNA methyltransferases Dnmt3a and Dnmt3b in the central nervous system. *J. Neurosci. Res.* *79*, 734–746.
- Forsyth, J.K., and Lewis, D.A. (2017). Mapping the Consequences of Impaired Synaptic Plasticity in Schizophrenia through Development: An Integrative Model for Diverse Clinical Features. *Trends Cogn. Sci.* *21*, 760–778.
- Frye, R.E., Casanova, M.F., Fatemi, S.H., Folsom, T.D., Reutiman, T.J., Brown, G.L., Edelson, S.M., Slattery, J.C., and Adams, J.B. (2016). Neuropathological Mechanisms of Seizures in Autism Spectrum Disorder. *Front. Neurosci.* *10*, 192. <https://doi.org/10.3389/fnins.2016.00192>.
- Gabel, H.W., Kinde, B., Stroud, H., Gilbert, C.S., Harmin, D.A., Kastan, N.R., Hemberg, M., Ebert, D.H., and Greenberg, M.E. (2015). Disruption of DNA-methylation-dependent long gene repression in Rett syndrome. *Nature* *522*, 89–93.
- Geaghan, M., and Cairns, M.J. (2015). MicroRNA and Posttranscriptional Dysregulation in Psychiatry. *Biol. Psychiatry* *78*, 231–239.
- Gigek, C.O., Chen, E.S., and Smith, M.A.C. (2016). Methyl-CpG-Binding Protein (MBD) Family: Epigenomic Read-Outs Functions and Roles in Tumorigenesis and Psychiatric Diseases. *J. Cell. Biochem.* *117*, 29–38.
- Griffiths-Jones, S., Grocock, R.J., van Dongen, S., Bateman, A., and Enright, A.J. (2006). miRBase: microRNA sequences, targets and gene nomenclature. *Nucleic Acids Res.* *34*, D140–D144.
- Grimson, A., Farh, K.K.-H., Johnston, W.K., Garrett-Engle, P., Lim, L.P., and Bartel, D.P. (2007). MicroRNA targeting specificity in mammals: determinants beyond seed pairing. *Mol. Cell* *27*, 91–105.
- Guo, J.U., Su, Y., Shin, J.H., Shin, J., Li, H., Xie, B., Zhong, C., Hu, S., Le, T., Fan, G., et al. (2014). Distribution, recognition and regulation of non-CpG methylation in the adult mammalian brain. *Nat. Neurosci.* *17*, 215–222.
- Hagerman, R.J., Berry-Kravis, E., Hazlett, H.C., Bailey, D.B., Jr., Moine, H., Kooy, R.F., Tassone, F., Gantois, I., Sonenberg, N., Mandel, J.L., and Hagerman, P.J. (2017). Fragile X syndrome. *Nat. Rev. Dis. Primers* *3*, 17065.
- Hatten, M.E., and Roussel, M.F. (2011). Development and cancer of the cerebellum. *Trends Neurosci.* *34*, 134–142.
- He, Y., and Ecker, J.R. (2015). Non-CG Methylation in the Human Genome. *Annu. Rev. Genomics Hum. Genet.* *16*, 55–77.
- Hébert, S.S., Horré, K., Nicolai, L., Papadopoulou, A.S., Mandemakers, W., Si-lahtaroglu, A.N., Kauppinen, S., Delacourte, A., and De Strooper, B. (2008). Loss of microRNA cluster miR-29a/b-1 in sporadic Alzheimer's disease correlates with increased BACE1/beta-secretase expression. *Proc. Natl. Acad. Sci. USA* *105*, 6415–6420.
- Hüfner, K., Frajo-Apor, B., and Hofer, A. (2015). Neurology issues in schizophrenia. *Curr. Psychiatry Rep.* *17*, 32.
- Jiang, X., and Nardelli, J. (2016). Cellular and molecular introduction to brain development. *Neurobiol. Dis.* *92* (Pt A), 3–17.
- Juzwik, C.A., Drake, S.S., Zhang, Y., Paradis-Isler, N., Sylvester, A., Amar-Zifkin, A., Douglas, C., Morquette, B., Moore, C.S., and Fournier, A.E. (2019). microRNA dysregulation in neurodegenerative diseases: A systematic review. *Prog. Neurobiol.* *182*, 101664.
- Keown, C.L., Berletch, J.B., Castanon, R., Nery, J.R., Disteche, C.M., Ecker, J.R., and Mukamel, E.A. (2017). Allele-specific non-CG DNA methylation marks domains of active chromatin in female mouse brain. *Proc. Natl. Acad. Sci. USA* *114*, E2882–E2890.
- Khanna, S., Rink, C., Ghoorkhanian, R., Gnyawali, S., Heigel, M., Wijesinghe, D.S., Chalfant, C.E., Chan, Y.C., Banerjee, J., Huang, Y., et al. (2013). Loss of miR-29b following acute ischemic stroke contributes to neural cell death and infarct size. *J. Cereb. Blood Flow Metab.* *33*, 1197–1206.

- Kinde, B., Gabel, H.W., Gilbert, C.S., Griffith, E.C., and Greenberg, M.E. (2015). Reading the unique DNA methylation landscape of the brain: Non-CpG methylation, hydroxymethylation, and MeCP2. *Proc. Natl. Acad. Sci. USA* *112*, 6800–6806.
- Knight, E.R.W., Patel, E.Y., Flowers, C.A., Crowther, A.J., Ting, J.P., Miller, C.R., Gershon, T.R., and Deshmukh, M. (2015). ASC deficiency suppresses proliferation and prevents medulloblastoma incidence. *Oncogene* *34*, 394–402.
- Kriegel, A.J., Liu, Y., Fang, Y., Ding, X., and Liang, M. (2012). The miR-29 family: genomics, cell biology, and relevance to renal and cardiovascular injury. *Physiol. Genomics* *44*, 237–244.
- Langmead, B., Trapnell, C., Pop, M., and Salzberg, S.L. (2009). Ultrafast and memory-efficient alignment of short DNA sequences to the human genome. *Genome Biol.* *10*, R25.
- Lavery, L.A., and Zoghbi, H.Y. (2019). The distinct methylation landscape of maturing neurons and its role in Rett syndrome pathogenesis. *Curr. Opin. Neurobiol.* *59*, 180–188.
- Lei, X., Lei, L., Zhang, Z., Zhang, Z., and Cheng, Y. (2015). Downregulated miR-29c correlates with increased BACE1 expression in sporadic Alzheimer's disease. *Int. J. Clin. Exp. Pathol.* *8*, 1565–1574.
- Li, H., Handsaker, B., Wysoker, A., Fennell, T., Ruan, J., Homer, N., Marth, G., Abecasis, G., and Durbin, R.; 1000 Genome Project Data Processing Subgroup (2009). The Sequence Alignment/Map format and SAMtools. *Bioinformatics* *25*, 2078–2079.
- Li, H., Mao, S., Wang, H., Zen, K., Zhang, C., and Li, L. (2014). MicroRNA-29a modulates axon branching by targeting doublecortin in primary neurons. *Protein Cell* *5*, 160–169.
- Lister, R., Mukamel, E.A., Nery, J.R., Urich, M., Puddifoot, C.A., Johnson, N.D., Lucero, J., Huang, Y., Dwork, A.J., Schultz, M.D., et al. (2013). Global epigenomic reconfiguration during mammalian brain development. *Science* *341*, 1237905.
- Liu, K., Xu, C., Lei, M., Yang, A., Loppnau, P., Hughes, T.R., and Min, J. (2018a). Structural basis for the ability of MBD domains to bind methyl-CG and TG sites in DNA. *J. Biol. Chem.* *293*, 7344–7354.
- Liu, Z., Li, Z., Zhi, X., Du, Y., Lin, Z., and Wu, J. (2018b). Identification of De Novo DNMT3A Mutations That Cause West Syndrome by Using Whole-Exome Sequencing. *Mol. Neurobiol.* *55*, 2483–2493.
- Lombardi, L.M., Baker, S.A., and Zoghbi, H.Y. (2015). MECP2 disorders: from the clinic to mice and back. *J. Clin. Invest.* *125*, 2914–2923.
- Long, J., Wang, Y., Wang, W., Chang, B.H.J., and Danesh, F.R. (2011). MicroRNA-29c is a signature microRNA under high glucose conditions that targets Sprouty homolog 1, and its in vivo knockdown prevents progression of diabetic nephropathy. *J. Biol. Chem.* *286*, 11837–11848.
- Love, M.I., Huber, W., and Anders, S. (2014). Moderated estimation of fold change and dispersion for RNA-seq data with DESeq2. *Genome Biol.* *15*, 550.
- Luo, C., Lancaster, M.A., Castanon, R., Nery, J.R., Knoblich, J.A., and Ecker, J.R. (2016). Cerebral Organoids Recapitulate Epigenomic Signatures of the Human Fetal Brain. *Cell Rep.* *17*, 3369–3384.
- Luo, C., Keown, C.L., Kurihara, L., Zhou, J., He, Y., Li, J., Castanon, R., Lucero, J., Nery, J.R., Sandoval, J.P., et al. (2017). Single-cell methylomes identify neuronal subtypes and regulatory elements in mammalian cortex. *Science* *357*, 600–604.
- Margis, R., Margis, R., and Rieder, C.R. (2011). Identification of blood microRNAs associated to Parkinson's disease. *J. Biotechnol.* *152*, 96–101.
- Martin, M. (2011). Cutadapt removes adapter sequences from high-throughput sequencing reads. *EMBnet.journal* *17*, 10–12.
- McKiernan, R.C., Jimenez-Mateos, E.M., Bray, I., Engel, T., Brennan, G.P., Sano, T., Michalak, Z., Moran, C., Delanty, N., Farrell, M., et al. (2012). Reduced mature microRNA levels in association with dicer loss in human temporal lobe epilepsy with hippocampal sclerosis. *PLoS ONE* *7*, e35921.
- McTague, A., Howell, K.B., Cross, J.H., Kurian, M.A., and Scheffer, I.E. (2016). The genetic landscape of the epileptic encephalopathies of infancy and childhood. *Lancet Neurol.* *15*, 304–316.
- Miller, B.H., Zeier, Z., Xi, L., Lanz, T.A., Deng, S., Strathmann, J., Willoughby, D., Kenny, P.J., Elsworth, J.D., Lawrence, M.S., et al. (2012). MicroRNA-132 dysregulation in schizophrenia has implications for both neurodevelopment and adult brain function. *Proc. Natl. Acad. Sci. USA* *109*, 3125–3130.
- Mo, A., Mukamel, E.A., Davis, F.P., Luo, C., Henry, G.L., Picard, S., Urich, M.A., Nery, J.R., Sejnowski, T.J., Lister, R., et al. (2015). Epigenomic Signatures of Neuronal Diversity in the Mammalian Brain. *Neuron* *86*, 1369–1384.
- Moore, L.D., Le, T., and Fan, G. (2013). DNA methylation and its basic function. *Neuropsychopharmacology* *38*, 23–38.
- Pandi, G., Nakka, V.P., Dharap, A., Roopra, A., and Vemuganti, R. (2013). MicroRNA miR-29c down-regulation leading to de-repression of its target DNA methyltransferase 3a promotes ischemic brain damage. *PLoS ONE* *8*, e58039.
- Papadopoulou, A.S., Serneels, L., Achsel, T., Mandemakers, W., Callaerts-Vegh, Z., Dooley, J., Lau, P., Ayoubi, T., Radaelli, E., Spinazzi, M., et al. (2015). Deficiency of the miR-29a/b-1 cluster leads to ataxic features and cerebellar alterations in mice. *Neurobiol. Dis.* *73*, 275–288.
- Patro, R., Duggal, G., Love, M.I., Irizarry, R.A., and Kingsford, C. (2017). Salmon provides fast and bias-aware quantification of transcript expression. *Nat. Methods* *14*, 417–419.
- Petri, R., Malmqvist, J., Fasching, L., Åkerblom, M., and Jakobsson, J. (2014). miRNAs in brain development. *Exp. Cell Res.* *321*, 84–89.
- Piñero, J., Bravo, À., Queralt-Rosinach, N., Gutiérrez-Sacristán, A., Deu-Pons, J., Centeno, E., García-García, J., Sanz, F., and Furlong, L.I. (2017). DisGeNET: a comprehensive platform integrating information on human disease-associated genes and variants. *Nucleic Acids Res.* *45* (D1), D833–D839.
- Qi, L., Hongjuan, H., Ning, G., Zhengbin, H., Yanjiang, X., Tiebo, Z., Zhijun, H., and Qiong, W. (2013). miR-370 is stage-specifically expressed during mouse embryonic development and regulates Dnmt3a. *FEBS Lett.* *587*, 775–781.
- Raudvere, U., Kolberg, L., Kuzmin, I., Arak, T., Adler, P., Peterson, H., and Vilo, J. (2019). g:Profiler: a web server for functional enrichment analysis and conversions of gene lists (2019 update). *Nucleic Acids Res.* *47* (W1), W191–W198.
- Ripa, R., Dolfi, L., Terrigno, M., Pandolfini, L., Savino, A., Arcucci, V., Groth, M., Terzibas Tozzini, E., Baumgart, M., and Cellerino, A. (2017). MicroRNA miR-29 controls a compensatory response to limit neuronal iron accumulation during adult life and aging. *BMC Biol.* *15*, 9.
- Rizzardi, L.F., Hickey, P.F., Rodríguez DiBlasi, V., Tryggvadóttir, R., Callahan, C.M., Idrizi, A., Hansen, K.D., and Feinberg, A.P. (2019). Neuronal brain-region-specific DNA methylation and chromatin accessibility are associated with neuropsychiatric trait heritability. *Nat. Neurosci.* *22*, 307–316.
- Roshan, R., Shridhar, S., Sarangdhar, M.A., Banik, A., Chawla, M., Garg, M., Singh, V.P., and Pillai, B. (2014). Brain-specific knockdown of miR-29 results in neuronal cell death and ataxia in mice. *RNA* *20*, 1287–1297.
- Samaco, R.C., Mandel-Brehm, C., McGraw, C.M., Shaw, C.A., McGill, B.E., and Zoghbi, H.Y. (2012). Crh and Oprm1 mediate anxiety-related behavior and social approach in a mouse model of MECP2 duplication syndrome. *Nat. Genet.* *44*, 206–211.
- Santarelli, D.M., Beveridge, N.J., Tooney, P.A., and Cairns, M.J. (2011). Upregulation of dicer and microRNA expression in the dorsolateral prefrontal cortex Brodmann area 46 in schizophrenia. *Biol. Psychiatry* *69*, 180–187.
- Schratt, G.M., Tuebing, F., Nigh, E.A., Kane, C.G., Sabatini, M.E., Kiebler, M., and Greenberg, M.E. (2006). A brain-specific microRNA regulates dendritic spine development. *Nature* *439*, 283–289.
- Siegert, S., Seo, J., Kwon, E.J., Rudenko, A., Cho, S., Wang, W., Flood, Z., Martorell, A.J., Ericsson, M., Mungenast, A.E., and Tsai, L.-H. (2015). The schizophrenia risk gene product miR-137 alters presynaptic plasticity. *Nat. Neurosci.* *18*, 1008–1016.
- Stark, K.L., Xu, B., Bagchi, A., Lai, W.S., Liu, H., Hsu, R., Wan, X., Pavlidis, P., Mills, A.A., Karayiorgou, M., and Gogos, J.A. (2008). Altered brain microRNA biogenesis contributes to phenotypic deficits in a 22q11-deletion mouse model. *Nat. Genet.* *40*, 751–760.
- Stiles, J., and Jernigan, T.L. (2010). The basics of brain development. *Neuropsychol. Rev.* *20*, 327–348.

- Stroud, H., Su, S.C., Hrvatin, S., Greben, A.W., Renthal, W., Boxer, L.D., Nagy, M.A., Hochbaum, D.R., Kinde, B., Gabel, H.W., and Greenberg, M.E. (2017). Early-Life Gene Expression in Neurons Modulates Lasting Epigenetic States. *Cell* **171**, 1151–1164.e16.
- Sun, E., and Shi, Y. (2015). MicroRNAs: Small molecules with big roles in neurodevelopment and diseases. *Exp. Neurol.* **268**, 46–53.
- Szklarczyk, D., Franceschini, A., Kuhn, M., Simonovic, M., Roth, A., Minguéz, P., Doerks, T., Stark, M., Müller, J., Bork, P., et al. (2011). The STRING database in 2011: functional interaction networks of proteins, globally integrated and scored. *Nucleic Acids Res.* **39**, D561–D568.
- Tatton-Brown, K., Seal, S., Ruark, E., Harmer, J., Ramsay, E., Del Vecchio Duarte, S., Zachariou, A., Hanks, S., O'Brien, E., Aksglaede, L., et al.; Childhood Overgrowth Consortium (2014). Mutations in the DNA methyltransferase gene DNMT3A cause an overgrowth syndrome with intellectual disability. *Nat. Genet.* **46**, 385–388.
- Toga, A.W., Thompson, P.M., and Sowell, E.R. (2006). Mapping brain maturation. *Trends Neurosci.* **29**, 148–159.
- Tonacci, A., Bagnato, G., Pandolfo, G., Billeci, L., Sansone, F., Conte, R., and Gangemi, S. (2019). MicroRNA Cross-Involvement in Autism Spectrum Disorders and Atopic Dermatitis: A Literature Review. *J. Clin. Med.* **8**, 88.
- Xi, Y., and Li, W. (2009). BSMAP: whole genome bisulfite sequence MAPping program. *BMC Bioinformatics* **10**, 232.
- Xi, J., Wu, Y., Li, G., Ma, L., Feng, K., Guo, X., Jia, W., Wang, G., Yang, G., Li, P., and Kang, J. (2017). Mir-29b Mediates the Neural Tube versus Neural Crest Fate Decision during Embryonic Stem Cell Neural Differentiation. *Stem Cell Reports* **9**, 571–586.
- Xie, W., Barr, C.L., Kim, A., Yue, F., Lee, A.Y., Eubanks, J., Dempster, E.L., and Ren, B. (2012). Base-resolution analyses of sequence and parent-of-origin dependent DNA methylation in the mouse genome. *Cell* **148**, 816–831.
- Xu, H., Sun, J., Shi, C., Sun, C., Yu, L., Wen, Y., Zhao, S., Liu, J., Xu, J., Li, H., et al. (2015). miR-29s inhibit the malignant behavior of U87MG glioblastoma cell line by targeting DNMT3A and 3B. *Neurosci. Lett.* **590**, 40–46.
- Xu, B., Cao, J., Zhang, J., Jia, S., Wu, S., Mo, K., Wei, G., Liang, L., Miao, X., Bekker, A., and Tao, Y.-X. (2017). Role of MicroRNA-143 in Nerve Injury-Induced Upregulation of Dnmt3a Expression in Primary Sensory Neurons. *Front. Mol. Neurosci.* **10**, 350.
- Yang, D., Wang, G., Zhu, S., Liu, Q., Wei, T., Leng, Y., Duan, T., and Kang, J. (2014). MiR-495 suppresses mesendoderm differentiation of mouse embryonic stem cells via the direct targeting of Dnmt3a. *Stem Cell Res. (Amst.)* **12**, 550–561.
- Yuen, R.K.C., Merico, D., Cao, H., Pellecchia, G., Alipanahi, B., Thiruvahindrapuram, B., Tong, X., Sun, Y., Cao, D., Zhang, T., et al. (2016). Genome-wide characteristics of *de novo* mutations in autism. *NPJ Genom. Med.* **1**, 160271–1602710.

STAR★METHODS

KEY RESOURCES TABLE

REAGENT or RESOURCE	SOURCE	IDENTIFIER
Antibodies		
Rabbit polyclonal anti-DNMT3A	Abcam	Cat# ab2850, RRID:AB_303355
Mouse monoclonal anti-beta-Actin	Sigma-Aldrich	Cat# A5316, RRID:AB_476743
Alexa Fluor 790-AffiniPure Goat Anti-Rabbit IgG (H+L)	Jackson ImmunoResearch Labs	Cat# 111-655-144, RRID:AB_2338086
Alexa Fluor 680-AffiniPure Goat Anti-Mouse IgG (H+L)	Jackson ImmunoResearch Labs	Cat# 115-625-146, RRID:AB_2338935
Rabbit polyclonal anti-cleaved-Caspase-3	Biocare Medical	Cat# CP229C
Mouse monoclonal anti-NeuN	Millipore	Cat# MAB377, RRID:AB_2298772
Mouse monoclonal anti-PCNA (PC10)	Cell Signaling Technology	Cat# 2586, RRID:AB_2160343
Rabbit monoclonal anti-27 Kip1 (D69C12)	Cell Signaling Technology	Cat# 3686, RRID:AB_2077850
Mouse monoclonal anti-DNMT3A	Abcam	Cat# ab13888, RRID:AB_300714
Dako EnVision+ System- HRP Labeled Polymer antibody	Agilent	Cat# K4001, RRID:AB_2827819
Cy5-Labeled Anti-Mouse IgG (H+L) RbSA	KPL	Cat# 072-02-18-18
Alexa Fluor 555 Goat anti-Rabbit IgG (H+L)	Molecular Probes	Cat# A-21429, RRID:AB_2535850
Chemicals, peptides, and recombinant proteins		
Kainic acid monohydrate	Sigma-Aldrich	Cat# K0250, CAS: 58002-62-3
Critical commercial assays		
miRNeasy Mini Kit	QIAGEN	Cat# 217004
Direct-Zol RNA mini-prep kit	Zymo Research	Cat# R2051
High-Capacity cDNA Reverse Transcription Kit	Applied Biosystems	Cat# 4368814
Power Up SYBR green master mix	Applied Biosystems	Cat# A25779
DNeasy Blood & Tissue Kit	QIAGEN	Cat# 69504
EZ DNA Methylation-Gold	Zymo Research	Cat# D5005
TruSeq Stranded mRNA Library Prep kit	Illumina	Cat# 20020594
Stranded RNA-Seq Kit	KAPA Biosystems	Cat# KK8401
Deposited data		
Cortical gene expression data from miR-29 ^{Nestin} and dnmt3a ^{mi5} mice	This paper	GEO: GSE140163 GEO: GSE157841
Amygdala gene expression data from MeCP2-deficient mice	Samaco et al., 2012	GEO: GSE33457
Hypothalamic gene expression data from MeCP2-deficient mice	Chahrour et al., 2008	GEO: GSE11150
Experimental models: organisms/strains		
mouse: miR-29ab1 ^{ff} , miR-29b2c ^{ff}	This paper	N/A
mouse: dnmt3a ^{mi5}	This paper	N/A
mouse: B6.C-Tg(CMV-cre)1Cgn/J	Jackson Laboratories	Cat# 006054
mouse: B6.Cg-Tg(Nes-cre)1Kln/J	Jackson Laboratories	Cat# 003771
Oligonucleotides		
poly(A) adaptor RT-PCR primer: GCGAGC ACAGAATTAATACGACTCACTATAGGT TTTTTTTTTTVN	This paper	N/A

(Continued on next page)

<i>Continued</i>		
REAGENT or RESOURCE	SOURCE	IDENTIFIER
universal reverse qPCR primer: GCGAGCACAGAATTAATACGAC	This paper	N/A
microRNA-specific forward qPCR primers for mir-29b: TAGCACCATTGAAATCAGT	This paper	N/A
U6 Forward qPCR primer: CGCTTCGGCAGCACATATAC	Long et al., 2011	N/A
U6 Reverse qPCR primer: AAAATATGGAACGCTTCACGA	Long et al., 2011	N/A
U6 snRNA TaqMan microRNA Control Assay	Thermo Fisher Scientific	Cat# 4427975 Assay ID 001973
hsa-miR-29a TaqMan microRNA Control Assay	Thermo Fisher Scientific	Cat# 4427975 Assay ID 002112
hsa-miR-29b TaqMan microRNA Control Assay	Thermo Fisher Scientific	Cat# 4427975 Assay ID 000413
hsa-miR-29c TaqMan microRNA Control Assay	Thermo Fisher Scientific	Cat# 4427975 Assay ID 000587
mGapdh forward qPCR primer: TGTGTCCGTCGTGGATCTGA	Knight et al., 2015	N/A
mGapdh reverse qPCR primer: CCTGCTTCACCACCTTCTTGA	Knight et al., 2015	N/A
mDnmt1 forward qPCR primer: CATGCTGCTTCCGCTTGC	This paper	N/A
mDnmt1 reverse qPCR primer: CTTTCCAAGTCTTTGAGCCGCC	This paper	N/A
mDnmt3a forward qPCR primer: GCTTTGGCATTGGAGAGCTG	This paper	N/A
mDnmt3a reverse qPCR primer: GCTTCTCCACACACACCACT	This paper	N/A
mDnmt3b forward qPCR primer: GCTTGTGCCAGACCTTGAA	This paper	N/A
mDnmt3b reverse qPCR primer: GTCTCCCTCATTGTTTCTGA	This paper	N/A
<i>Software and algorithms</i>		
Prism v8.3.1	GraphPad	https://www.graphpad.com:443/
R v3.5.1	R Core Team	https://www.R-project.org
TargetScan v.5.2 & v7.2	Grimson et al., 2007	http://www.targetscan.org/mmu_72/
miRBase v.18	Griffiths-Jones et al., 2006	http://www.mirbase.org/
Samtools v1.2	Li et al., 2009	https://github.com/samtools/samtools
Bowtie v1.1.1	Langmead et al., 2009	http://bowtie-bio.sourceforge.net/
STRING v.9.0	Szklarczyk et al., 2011	https://string-db.org/
Bsmap v2.74	Xi and Li, 2009	https://code.google.com/archive/p/bsmap/
Cutadapt	Martin, 2011	https://cutadapt.readthedocs.io/en/stable/
STAR	Dobin et al., 2013	https://code.google.com/archive/p/rna-star/
Salmon	Patro et al., 2017	https://github.com/COMBINE-lab/salmon
DESeq2	Love et al., 2014	http://www.bioconductor.org/packages/release/bioc/html/DESeq2.html
gProfiler	Raudvere et al., 2019	https://biit.cs.ut.ee/gprofiler/
Reactome	Fabregat et al., 2018	https://reactome.org
DisGeNET	Piñero et al., 2017	https://www.disgenet.org/

(Continued on next page)

Continued

REAGENT or RESOURCE	SOURCE	IDENTIFIER
Aperio ImageScope v12.3.3	LeicaBiosystems	https://www.leicabiosystems.com/digital-pathology/manage/aperio-imagescope/
7500 System SDS v1.4	Applied Biosystems	https://www.thermofisher.com/us/en/home/technical-resources/software-downloads/applied-biosystems-7500-real-time-pcr-system.html
QuantStudio Design and Analysis Software v1.5	Applied Biosystems	https://www.thermofisher.com/us/en/home/global/forms/life-science/quantstudio-3-5-software.html
Image Studio acquisition software v4.0	Li-Cor	https://www.licor.com/bio/image-studio/resources

RESOURCE AVAILABILITY

Lead contact

Further information and requests for resources and reagents should be directed to and will be fulfilled by the Lead Contact, Mohanish Deshmukh (mohanish@med.unc.edu).

Materials availability

All unique reagents generated in this study are available from the Lead Contact without restriction.

Data and code availability

The accession numbers for the sequencing data reported in this paper have been deposited in Gene Expression Omnibus (GEO): GSE140163, GSE157841.

EXPERIMENTAL MODEL AND SUBJECT DETAILS

All animal handling and experiments were carried out in accordance with the National Institutes of Health Guide for Care and Use of Laboratory Animals and as approved by the Animal Care and Use Committee of the University of North Carolina (UNC).

Mice were housed 2-5 per cage in a 12 h light, 12 h dark cycle. Food and water were provided *ad libitum*. Cohorts were composed of animals of both sexes, aged as indicated in figure legends. Control mice (wild-type) were wild-type littermates of mutant mice.

The miR-29ab1^{ff}, miR-29b2c^{ff} mice were generated in the 129/SvEv background. The Dnmt3a^{mi5} knock-in mice were in the C57BL/6J background.

METHOD DETAILS

Generation of knock-out and knock-in mice

The miR-29ab1 and miR-29b2c floxed alleles were generated by the Duke Transgenic Mouse Facility by homologous recombination and genomic targeting. An 827 bp or an 817 bp genomic segment containing respectively, miR-29a and miR-29b1, or miR-29b2 and miR-29c, were amplified from 129/SvEv mouse genomic DNA. To amplify the long arm (LA) and short arm (SA), a BAC clone (RP24-248C11 for miR-29ab1 and RP23-465H4 for miR-29b2c) was used as PCR template. miR-29ab1 or miR-29b2c gene segments and their corresponding LA and SA were cloned into the PGKneoF2L2DTA targeting vector. After verification for the absence of mutation, targeting vectors were linearized by SacII (New England BioLabs) restriction enzyme digestion and were used for microinjection of ES cells from 129/SvEv-B6 mice. ES cells were positively selected in neomycin-containing medium, and successful genomic targeting was confirmed by PCR. Animals were bred and maintained in the SPF facility managed by Duke University Division of Laboratory Animal Research. All animal procedures were approved by the Duke University Institutional Animal Care and Use Committee.

The above mice were bred to generate mice floxed at both genomic loci (miR-29ab1^{ff}, miR-29b2c^{ff} mice). Deletion of miR-29 was carried out by crossing the above mice with various Cre recombinase lines including CMV-Cre and Nestin-Cre (Jackson Laboratories, #006054 and #003771) to obtain miR-29^{CMV} and miR-29^{Nestin} knock-out mice.

The knock-in mouse with five miR-29-binding sites mutated in *Dnmt3a* 3' UTR (Dnmt3a^{mi5} mice) was generated by the UNC Animal Models Core Facility by CRISPR/Cas9 nuclease technology. CRISPR guide RNAs were designed to cut at miR-29-binding site 1 and miR-29-binding site 5 (target sequence miR-29-1: ACATCCCCGACTTCATAA; target sequence miR-29-5: GAGGAATTAGCAC-CAGCT). A donor vector with approximately 1 kb homology arms flanking the 2909 bp region encompassing the 5 miR-29-binding

sites, all mutated from TGGTGCT to CACGGCT, was generated. Guide RNAs, Cas9 protein and donor vector were injected into C57BL/6J mouse embryos. Founders were screened for homologous integration of the five mutated miR-29-binding sites.

Small RNA sequencing and analysis

Total RNA was extracted from P18 and P250 wild-type CD-1 mouse cerebellum using miRNeasy kit (QIAGEN, #217004). Libraries were prepared using a modification of the TruSeq protocol. Briefly, 1 μ g total RNA was ligated to 3 pmol of 3' linker using T4 RNA ligase 2. RNA size fractions corresponding to 35–70 nucleotides (insert plus linker) were isolated on gel and ligated to 3 pmol of 5' linker. Products were reverse transcribed, PCR amplified to mid-log phase, and size isolated. Libraries were barcoded using indexed 5' linkers before single end sequencing at the High Throughput Genomic Sequencing Facility at UNC Chapel Hill on an Illumina HiSeq 2000 (50 cycles). Small RNA sequencing reads were processed using miRquant (Baran-Gale et al., 2013). MiRquant is a small RNA-sequencing pipeline that involves trimming, alignment to the mouse genome (mm9), miRNA and iso-miRNA assignment of the reads according to miRbase annotations (v18), quantification and normalization to reads per million reads mapped, and differential expression analysis. The filter applied included only those miRNA for which reads per million (RPM) was > 50 in the P250 sample.

RT-qPCR analysis

For miRNA RT-qPCR, total RNA was extracted from mouse cortex and cerebellum using miRNeasy kit (QIAGEN, #217004). RNA (10 ng) was reverse transcribed using Superscript III reverse transcriptase (Invitrogen) and specific RT primers for mature miR-29a, miR-29b, miR-29c and U6 RNA (TaqMan MicroRNA Assays, Applied Biosystems). Real-time PCR was carried out with an ABI7500 thermocycler (Applied Biosystems) and relative quantification was estimated using the $\Delta\Delta$ Ct method. Sample variability was corrected by normalizing to U6 RNA levels.

Alternatively, total RNA was extracted from mouse cortex with TRI reagent. Tissues were homogenized in TRI reagent (Zymo Research), RNA was separated with chloroform and precipitated with an equal volume of isopropanol. Total RNA (1 μ g) was poly-adenylated with recombinant Poly(A) Polymerase (1.2 U per 20 μ l reaction) for 1 h at 37°C. RT-PCR reactions were performed using High-Capacity cDNA Reverse Transcription Kit (Applied Biosystems) with a poly(A) adaptor PCR primer (GCGAGCACA-GAATTAATACGACTCACTATAGGTTTTTTTTTTTTVN) (adapted from Biggar et al., 2014). Real-time PCR reactions were run using microRNA-specific forward primers (mir-29b: TAGCACCATTGAAATCAGT), a universal reverse primer (GCGAGCACAGAATTAATACGAC) and Power Up SYBR green master mix (Applied Biosystems) on a QuantStudio 3 thermocycler (Applied Biosystems). Relative quantification was estimated using the $\Delta\Delta$ Ct method and U6 (U6 Forward: CGCTTCGGCAGCACATATAC; U6 Reverse: AAAATATGGAACGCTTCACGA) to normalize each miRNA relative level.

For analysis of *Dnmt1*, *Dnmt3a* and *Dnmt3b* mRNA, cDNA libraries were prepared using High-Capacity cDNA Reverse Transcription Kit (Applied Biosystems) from total RNA (1 μ g) extracted from mouse cortex and cerebellum with TRI reagent. Primers were designed using the NCBI primer designing tool. The following primers were used: *mGapdh* forward: TGTGTCCGTCGTGGATCTGA; *mGapdh* reverse: CCTGCTTCACCACCTTCTTGA; *mDnmt1* forward: CATGCTGCTTCCGCTTGC; *mDnmt1* reverse: CTTTCCAAGTCTTTGAGCCGCC; *mDnmt3a* forward: GCTTTGGCATTGGAGAGCTG; *mDnmt3a* reverse: GCTTCTCCACACACACACT; *mDnmt3b* forward: GCTTGTGCCAGACCTTGAA; *mDnmt3b* reverse: GTCTCCCTTCATTGTTTCCTGA. Real-time PCR reactions were performed with Power Up SYBR green master mix (Applied Biosystems) on a QuantStudio 3 thermocycler (Applied Biosystems). Relative quantification was estimated using the $\Delta\Delta$ Ct method and *Gapdh* to normalize each mRNA relative level.

Mouse behavioral analysis: hindlimb clasp

Adult mice, when suspended by the tail, extend their four limbs in anticipation of contact. Instead, mice with defects in various brain regions (i.e., cerebellum, basal ganglia, and neocortex) and the spinal cord display hindlimb clasp toward the abdomen. Each mouse was tail suspended for 90 s and monitored by video recording.

Grooming

Subject were placed and left undisturbed in a new standard mouse cage. Mice were recorded on video and repetitive self-grooming was measured over 30 minutes and expressed as the percentage of time spent grooming.

Open field test

Exploratory activity in a novel environment was assessed by a 60 min trial in an open field chamber (41 cm x 41 cm x 30 cm) crossed by a grid of photobeams (VersaMax system, AccuScan Instruments). Counts were taken of the number of photobeams broken during the trial in 5 min intervals, with separate measures for total distance traveled and fine movements (the repeated breaking of the same set of photobeams). Time spent in the center region of the open field was measured as an index of anxiety-like and risk-taking behavior.

Acoustic startle test

This procedure is based on the reflex whole-body flinch (startle response) that follows exposure to a sudden noise. Measures are taken of prepulse inhibition, which occurs when a weak pre-stimulus leads to a reduced startle in response to a subsequent louder noise. Subjects were tested with a SR-Lab system (San Diego Instruments). Mice were placed in a small Plexiglas cylinder within a

larger, sound-attenuating chamber. The cylinder was seated upon a piezoelectric transducer, which allowed vibrations to be quantified. The chamber included a ceiling light, fan, and a loudspeaker for the acoustic stimuli. Background sound levels (70 dB) and calibration of the acoustic stimuli were confirmed with a digital sound level meter (San Diego Instruments). The test began with a 5 min habituation period, followed by forty-two trials. There were seven different types of trials: no-stimulus trials, trials with acoustic startle stimulus alone (40 ms; 120 dB), and trials in which a prepulse stimulus (20 ms; either 74, 78, 82, 86, or 90 dB) occurred 100 ms before the acoustic startle stimulus. The levels of prepulse inhibition at each prepulse sound intensity was calculated as $100 - [(response\ amplitude\ for\ prepulse\ stimulus\ and\ startle\ stimulus\ together / response\ amplitude\ for\ startle\ stimulus\ alone) \times 100]$.

Wire-hang test for grip strength

At the start of the test, subjects were placed on a large metal cage lid. The lid was gently shaken to induce the mouse to grip onto the metal grid. The cage top was then flipped over, and latency for the mouse to fall from the lid was recorded during the 60 s test.

Rotarod test

Subjects were tested for motor coordination and learning on an accelerating rotarod (Ugo Basile, Stoelting Co.). On a first test session, mice were given three trials, with 45 s between each trial. An additional trial was given 48 h later. The initial speed was set at 3 rpm, with a progressive increase to a maximum of 30 rpm across a total 5 min trial. Measures were taken for latency to fall from the top of the rotating barrel.

Kainic acid-induced seizures scoring

Animals were injected intraperitoneally with 30 mg/kg of kainic acid (Sigma-Aldrich, #K0250) to induce seizures. Following kainic acid administration, mice were placed in a cage and video-recorded for 3 hours or until death was observed. The behavioral scores were as follows: 1: hypoactivity; 2: head nodding; 3: anterior clonus; 4: loss of balance or repeated falling; 5: severe tonic-clonic seizures; 6, jumping; 7: death.

Western blotting

Whole cortex was lysed by homogenization in RIPA buffer. Protein concentrations were quantified by bicinchoninic acid (BCA) assay (Pierce, #23225) and equal amounts of protein were resolved on 8% SDS-polyacrylamide gels before transfer onto Immobilon-FL PVDF membranes (Millipore). After blocking (TBS, 1% ovalbumin, 1% fish gelatin, 0.05% tween 20), membranes were probed with anti-DNMT3A (Abcam, #ab2850, 1:500) and anti- β Actin (Sigma-Aldrich, #A5316, 1:2,000) primary antibodies. Signals from infrared dye-conjugated secondary antibodies (Alexa Fluor 790 & 680, Jackson ImmunoResearch Inc., 1:10,000) were detected using an Odyssey CLx imager (LI-COR) and were quantified using Image Studio software (LI-COR). Regions of interest (ROIs) were drawn around bands of interest and the density was measured. Relative densities were normalized to housekeeping genes (β Actin) and calculated against the average of the WT samples on each membrane.

Whole genome bisulfite-sequencing

Genomic DNA was extracted from mouse cortex with the DNeasy Blood & Tissue Kit (QIAGEN) and sonicated with a Covaris S2 instrument to generate 200 bp fragments. Unmethylated lambda DNA (0.1%–0.5%; Promega D1521) was spiked in to assess conversion rates. Whole genome bisulfite-sequencing was performed similarly as described (Mo et al., 2015) except that the EZ DNA Methylation-Gold Kit (Zymo Research) was used for bisulfite conversion. Libraries were sequenced on a MiSeq system (Illumina) by performing a 75x2 cycle run. BSmap v.2.74 (Xi and Li, 2009) was used to map reads to the mm9 mouse genome assembly and only uniquely mapping reads were retained for analyses. Methylation levels were determined by calculating $\#C / (\#C + \#T)$ for the indicated cytosine pair (e.g., CG, CA, CT or CC), where $\#C$ is the number of C reads and $\#T$ is the number of T reads. All our libraries had less than 1% non-conversion rate assessed by unmethylated lambda DNA spiked into each sample (Tables S3 and S4). Methylation levels were summarized by gene (transcription start site through transcription termination site) using RefSeq gene annotations.

RNA sequencing and analysis

For miR-29^{Nestin} mice, total RNA was extracted from the cortex of P40 mice using RNeasy Mini Kit (QIAGEN). Stranded mRNA libraries were prepared with TruSeq Stranded mRNA Library Prep Kit (Illumina). Paired end sequencing (50 cycles) was performed on an Illumina HiSeq 2500 v4 (high output).

For Dnmt3a^{mi5} mice, total RNA was extracted from the cortex of 4.5 months old mice using Direct-Zol RNA mini-prep kit (Zymo Research, #R2051). Stranded mRNA libraries were prepared using the KAPA stranded mRNAseq kit (KAPA Biosystems). Libraries were dual barcoded before paired end sequencing (50 cycles) on an Illumina HiSeq 4000 (high output). All sequencing were performed at the High Throughput Genomic Sequencing Facility at UNC Chapel Hill. Reads were then trimmed and filtered of adaptor sequencing using cutadapt (Martin, 2011), and required to have at least 90% of bases with quality scores exceeding 20. Reads were then aligned to the reference human genome (hg19) using STAR (Dobin et al., 2013), and transcript abundance was estimated using Salmon (Patro et al., 2017). Differential expression between each genetic model and wild-type control was analyzed using DESeq2 (Love et al., 2014). Differentially expressed genes (adjusted p value < 0.1) were annotated for pathway (Reactome) (Fabregat et al.,

(2018) and disease (DisGeNET) (Piñero et al., 2017) enrichments using gProfiler (Raudvere et al., 2019). Enrichments with FDR < 0.05 were considered significant.

miRHub analysis

First, we used the seed-based target prediction algorithm TargetScan v.5.2 (Grimson et al., 2007) to determine for each miRNA the number of predicted conserved targets among the genes in our gene sets (genes found upregulated by RNA-seq with fold change > 0 and adjusted p value < 0.1). Each predicted miRNA-gene interaction was assigned a score based on the strength of the seed match, the level of conservation of the target site, and the clustering of target sites within that gene's 3' UTR. Finally, for each miRNA, the final targeting score was calculated by summing the scores across all genes and dividing by the number of genes. We repeated this procedure 10,000 times, with a new set of randomly selected mouse genes each time, in order to generate a background distribution of the predicted targeting scores for each miRNA. These score distributions were then used to calculate an empirical p value of the targeting score for each miRNA in our gene set. Genes were selected at random from a pool with similar overall connectivity to the genes in our gene set, and to account for differences in the average 3' UTR length between the genes of interest and the randomly selected genes in each simulation, the targeting score was normalized by 3' UTR length.

Immunohistochemistry staining

Mice were anesthetized using isoflurane and transcardially perfused with PBS followed by 4% paraformaldehyde. Brains were post-fixed in 4% paraformaldehyde overnight before paraffin-embedded sections were prepared. Hematoxylin-eosin (H&E) stains were done using an Autostainer XL (Leica Biosystems). Fluorescence (cleaved-Caspase-3, NeuN, PCNA and p27) and chromogenic (DNMT3A) immunohistochemistry were carried out in the Bond fully-automated slide staining system (Leica Microsystems) using .

Slides were dewaxed in Bond Dewax solution (Leica Biosystems, #AR9222) and hydrated in Bond Wash solution (Leica Biosystems, #AR9590). Heat-induced antigen retrieval was performed for 30 min at 100°C in Bond-Epitope Retrieval solution 1 pH-6.0 (Leica Biosystems, #AR9961, for NeuN, PCNA and p27 stainings) or solution2 pH-9.0 (Leica Biosystems, #AR9640, for cleaved-Caspase-3 and DNMT3A stainings). The antigen retrieval was followed with 5 min Bond peroxide blocking step (Leica Biosystems, #DS9800) and with 30 min with Rodent Block M (Biacare Medical, #RBM961L). After pretreatment, slides are incubated with primary antibody. Primary antibodies were as follows: anti-cleaved-Caspase-3 (Biacare Medical, #CP229C, Lot 110513, 1:200, 4 h), anti-NeuN (Millipore, #MAB377, lot NG1876252, 1:1000, 1 h), anti-PCNA (Cell Signaling Technology, #2586, 1:1000, 6h), anti-p27 (Cell Signaling Technology, #3686, 1:1000, 6h) and anti-DNMT3A (Abcam, #ab13888, lot GR222526, 1:100, 4 h).

For cleaved-Caspase-3 and NeuN, fluorescence detection was performed using Bond polymer Refine Detection kit (Leica Biosystems, #DS9800) and EnVision+ System- HRP labeled polymer anti-mouse (Dako, #K4001), respectively. For PCNA and p27, fluorescence detection was performed using Cy5-labeled anti-mouse IgG (KPL #072-02-18-18) and Alexa Fluor® 555 anti-rabbit IgG (Molecular Probes, #A-21429), respectively, and Bond Research Detection System (Leica Biosystems, #DS9455). Stained slides were counterstained with Hoechst 33258 (Invitrogen, #H3569) and mounted with ProLong Gold antifade reagent (Invitrogen, #P36934).

For DNMT3A, chromogenic detection was performed using EnVision+ System- HRP labeled polymer anti-mouse (Dako, #K4001) and Bond Intense R Detection System (Leica Biosystems, #DS9263). Stained slides were dehydrated and mounted.

Representative images from brains (n = 3) were acquired with Aperio ScanScope XT (Leica) using 20x objective. All staining and imaging were performed at the Translational Pathology Laboratory, UNC Chapel Hill.

QUANTIFICATION AND STATISTICAL ANALYSIS

For all experiments, the value *n* represents the number of independent animals used and can be found in the figure legends. No statistical methods were used to predetermine sample sizes which were estimated based on similar samples sizes reported in the literature. No sample was excluded from the analysis. All behavior studies were performed blind to genotype. Biochemical analysis were performed without blinding.

Data visualization and statistical analyses were performed using GraphPad Prism v.8.3.1 and R v.3.5.1. Bar and line graphs represent the mean ± SEM and box-and-whiskers plots depict the median and interquartile range (IQR, 25th and 75th percentiles) ± 1.5x IQR. For all dataset, normality was tested using the Shapiro-Wilk normality test. No data was excluded from any analysis. The statistical tests used are indicated in the figure legends. In particular, for all assays comparing two groups with normal data distributions, the Student's *t* test (unpaired, two-tailed) with a 95% confidence interval (CI) was performed. For multiple comparison tests, multiple unpaired *t* test with Holm-Sidak correction or one-way Analysis of Variance (ANOVA) with post hoc Dunnett's multiple comparisons test were performed. For behavioral assays based on repeated-measurements, data with normal distribution were analyzed using repeated-measures ANOVA with a 95% CI for the factor genotype, followed by a post hoc Sidak's multiple comparisons test. For samples with unequal sizes and/or variances, Welch's *t* test (two-tailed). For all data not normally distributed, the Mann Whitney test (two-tailed) with a 95% CI was used. For survival analysis, the Gehan-Breslow-Wilcoxon test was performed.